To: Undisclosed Recipients

From: Randy Lee, NASA Marshall Space Flight Center

Subject: Addendum to "C-C and CMC Composites for Space Telescope Platforms", SBIR contract NNXXXXXX, Phase II activity

Date: August 22, 2011

CC: Undisclosed Recipients

The following sections provide supplemental information regarding some of the tools and characterization methods that I have developed for the densification of ceramic matrix composites (CMC) and carbon-carbon (C-C) composite systems, particularly those which include silicon-based ceramic constituents derived from preceramic polymers. Hopefully, this information is worth scanning and might be beneficial in you work efforts.

Section I: Excepts from "Relationships in Carbon-Carbon Substrate Processing"

Section II: Excerpts from "Evaluation of C/C-SiC Composites for Small Motor Components"

Section III: Excerpts from "Density, Porosity & Constituent Fractions in C-C/SiC"

Section IV: Excerpts from "Density, Porosity & Constituent Fractions in C-C/SiC"

Section V: Excerpts from "Density, Porosity & Constituent Fractions in C-C/SiC"

Section VI: Excerpts from "Preceramic PolyCarbosilanes: Reactions & Mechanisms"

Please note that, while many of these techniques are now well established, all ideas, concepts and theories presented in the following sections are exclusively author's original handiwork, except where noted. No guarantee is given as to the correctness in wording and none is given regarding the accuracy or validity of any of the proposed methods or hypotheticals.

Best Regards,

Randy Lee
Sr. Materials Engineer
NASA Marshall Space Flight Center
randy.e.lee@nasa.gov

Section I (Phenolic Resin Densification)

Selected excepts taken from **"Relationships in Carbon-Carbon Substrate Processing"**, *Randy Lee*

The importance of characterizing substrate matrix weight fraction is especially crucial for C-C and CMC composites since the very nature of these material systems is based on the concept of *matrix densification*. There are now strong indications that a solid understanding of the a composite's matrix fraction and porosity at the fully densified state are the key properties in choosing the exact process methodologies for finishing operation, particularly those involving conversion coating concepts.

Graphical Analysis of Matrix Content and Other Parameters from the Table of Averages

Using precision values gathered for as-molded resin content, impregnation/cure weight gains, pyrolysis weight losses, and the model formulas derived above, matrix weight fraction m_{wi} at each carbon state up to ACC-4 is calculated and plotted below:

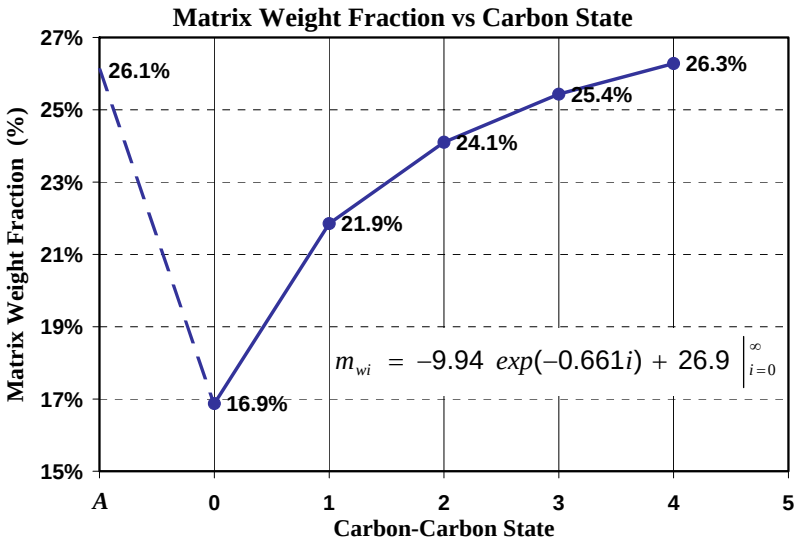

Other properties were evaluated and treated in a similar manner and their plots are given on the following page. Functional expressions for ρ_b, p, F (flexural strength) and I (interlaminar tensile or ILT strength) have been obtained and are included in each graph. In the same manner, it has been concluded that the $m_{wi} = ae^{-bi} + c$ expression most appropriately represents the *average* behavior of each property as it progresses through the densification process. As with the matrix weight fraction, the dashed line from state *A* to the first carbon state is not represented by the relationship but is included in the graphic for illustrative purposes only.

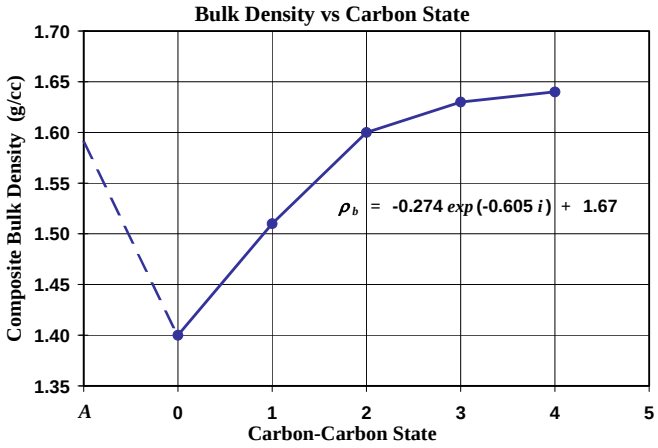
Bulk Density vs Carbon State
Composite Bulk Density (g/cc)
1.70
1.65
1.60
1.55
1.50
1.45
1.40
1.35
ρ_b = -0.274 exp (-0.605 i) + 1.67
A 0 1 2 3 4 5
Carbon-Carbon State

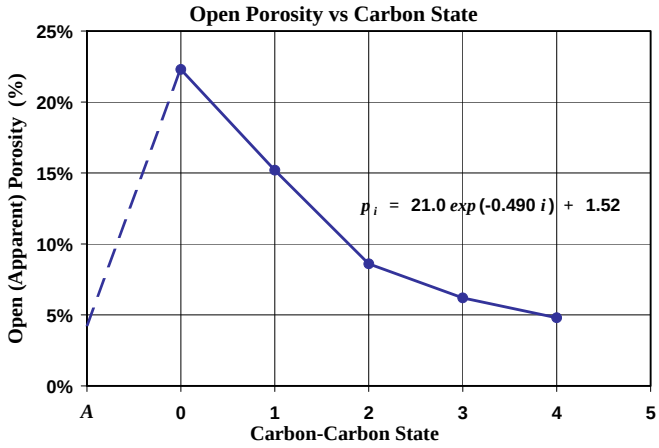
Open Porosity vs Carbon State
Open (Apparent) Porosity (%)
25%
20%
15%
10%
5%
0%
p_i = 21.0 exp (-0.490 i) + 1.52
A 0 1 2 3 4 5
Carbon-Carbon State

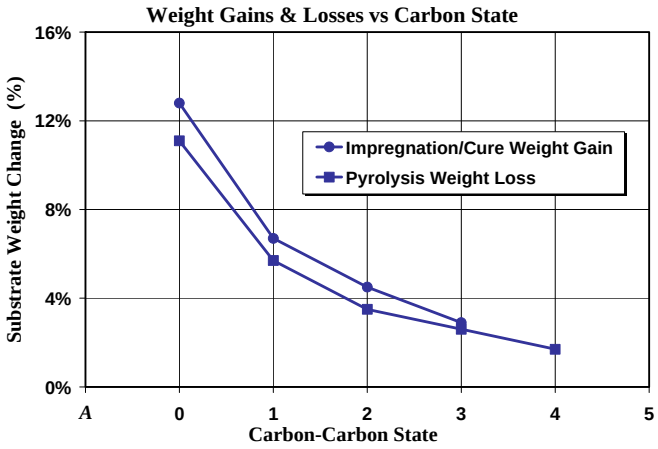
Weight Gains & Losses vs Carbon State
Substrate Weight Change (%)
16%
12%
8%
4%
0%
Impregnation/Cure Weight Gain
Pyrolysis Weight Loss
A 0 1 2 3 4 5
Carbon-Carbon State

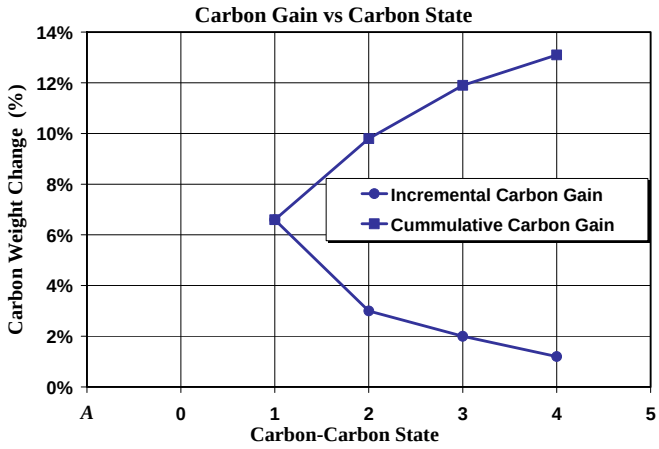
Carbon Gain vs Carbon State
Carbon Weight Change (%)
14%
12%
10%
8%
6%
4%
2%
0%
Incremental Carbon Gain
Cummulative Carbon Gain
A 0 1 2 3 4 5
Carbon-Carbon State

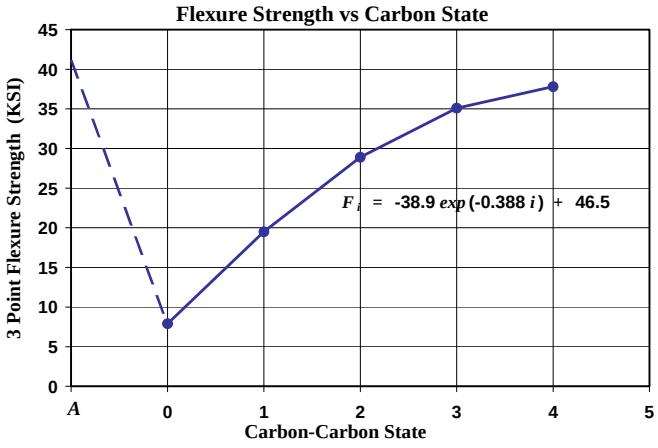
Flexure Strength vs Carbon State
3 Point Flexure Strength (KSI)
45
40
35
30
25
20
15
10
5
0
F_i = -38.9 exp (-0.388 i) + 46.5
A 0 1 2 3 4 5
Carbon-Carbon State

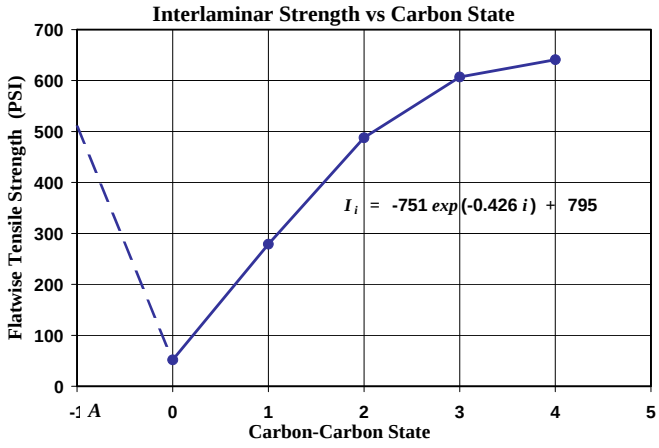
Interlaminar Strength vs Carbon State
Flatwise Tensile Strength (PSI)
700
600
500
400
300
200
100
0
I_i = -751 exp (-0.426 i) + 795
-1 A 0 1 2 3 4 5
Carbon-Carbon State

Section II (Preceramic SiC Densification)

Excerpts taken from **"Evaluation of C/C-SiC Composites for Small Motor Components"**, *Randy Lee*

Background:

At any point during the fabrication (or lifetime) of a composite substrate, the bulk density can be defined as the sum of the products of each constituent density and its respective volume fraction . . .

$$\rho_b = \frac{w_f + w_m}{V} = \frac{\rho_f v_f + \rho_m v_m}{V} = f_v \rho_f + m_v \rho_m$$

where w_f, w_m, v_f and v_m are the actual weights and volumes of the fiber and matrix phases comprising the slab, billet or article which has an actual weight and volume of W and V. Accordingly, ρ_f and ρ_m are the impervious fiber and matrix densities, and f_w, m_w, f_v, m_v and p are the fiber and matrix weight fractions, along with the fiber, matrix and porosity volume fractions respectively.

Here, it is realized that the total weight of a slab or panel is always equal to the sum of weights of all of its constituents while the total volume is always equal to the sum of volumes of all the constituents . . .

$$W = w_f + w_m \qquad \text{and} \qquad V = v_f + v_m + p$$

In these types of composites, both the physical weight and volume of the fiber are usually considered to be constant throughout the process while, the total matrix weight may itself be a sum of several components such as carbon, ceramic and/or resin . . . $w_m = w_c + w_{SiC} + w_r$

Also, the sum of fractions by weight and the sum of fractions by volume are always unity. Respectively . . .

$$f_w + m_w = 1 \qquad \text{and} \qquad f_v + m_v + p = 1$$

Fiber and matrix volume fractions can be expressed in terms of their respective weight fractions. Since . . .

$$\rho_f = \frac{w_f}{v_f} = \frac{f_w W}{f_v V} = \frac{f_w}{f_v}\rho_b \qquad \text{then . . .} \qquad f_v = f_w \frac{\rho_b}{\rho_f} = (1 - m_w)\frac{\rho_b}{\rho_f}$$

$$\text{Likewise . . .} \qquad m_v = m_w \frac{\rho_b}{\rho_m}$$

The true or real composite density (sometimes called the skeletal or impervious density) refers to the non-porous portion of the substrate (i.e... the fiber and matrix only). While the bulk density is defined by constituent volume fractions, the true composite density is a function of the weight fractions and approaches the bulk density when the pore volume approaches zero . . .

$$\rho_t = \frac{W}{v_f + v_m} = \frac{W}{V - v_p}$$

$$\rho_t = \rho_b (1 - p)^{-1}$$

With inclusion of the porosity fraction, the bulk density can be written in terms of component weight fractions. . .

(1A) $$\rho_b = \frac{W}{v_f + v_m + v_p} = \left(f_w \rho_f^{-1} + m_w \rho_{\mathrm{m}}^{-1} \right)^{-1} (1 - p)$$

Rearrangement of Eq(1A) gives an expression for estimating the porosity from the fiber density, matrix density and matrix content. This formula has come in very handy for numerous material systems over the years . . .

(2A) $$p = 1 - \rho_b \left[(1 - m_w) \rho_f^{-1} + m_w \rho_m^{-1} \right]$$

Now at the beginning of the densification process, the rigidized preform structure is pitch impregnated and then subjected to pyrolysis which converts the pitch material into a non-melting, pre-graphitc mesophase carbon. As ceramic densification commences, the slab undergoes sequential cycles of SMP-10 pre-ceramic polymer resin impregnation/cure followed by pyrolysis to convert the cured polymer into SiC ceramic (the slab is weighed before and after each step). The CMC densification process is defined essentially by three parameters: (1) the positive weight gain η_g that occurs when an article in a pyrolyzed state (i) is impregnated with polymer/resin to a bimatrix state (iB), and (2) the positive weight loss η_l that occurs due to pyrolysis of the article in a bimatrix (impregnated) state (iB) to the next corresponding ceramic state ($i+1$). These two parameters result in changes exclusively within the matrix and are represented respectfully by . . .

$$\eta_{g,i} = \frac{W_{iB} - W_i}{W_i} = \Delta m_{w,i \to iB} \qquad \text{and} \qquad \eta_{l,i+1} = \frac{W_{iB} - W_{i+1}}{W_{iB}} = \Delta m_{w,iB \to i+1}$$

bimatrix weight gain at state *i* to state *iB* — pyrolysis weight loss at state *iB* to state *i*+1

Each step in the process can be recognized by subscripts denoting the preform state $i = P$, the single carbon (C-C) state $i = 0$, any one of the subsequent ceramic (pyrolyzed) states, $i = 1, 2, 3, \ldots$, or one of the intermediate impregnated (bimatrix) states, $iB = 0B, 1B, 2B, \ldots$ At any given state in the process, the matrix will consist of one or more of the following: (1) a fixed level of inorganic pre-graphitic carbon (established during the initial pitch densification step); (2) previously deposited inorganic SiC ceramic (whose fraction cumulatively increases over the matrix densification process); and (3) unconverted pre-ceramic, semi-organic SMP polymer which has just been impregnated into the porosity of the composite. For the convenience of this discussion, the term 'bimatrix' will simply refer to one of the impregnated states prior to pyrolysis.

(3) The cumulative ceramic weight gain η_{SiC} from the initial ceramic (pyrolyzed) state to any future ceramic (pyrolyzed) state is the total converted ceramic matrix material deposited within the pores of the composite and represents the change in matrix content as the article progresses from the state $i = 0$ to the state i . . .

$$\eta_{SiC,0 \to i} = \frac{W_i - W_0}{W_0} = \Delta m_{w,0 \to i}$$

While the state $i = 0$ is actually the substrate's only carbon state, for convenience, the nomenclature used here may often refer to it as the first ceramic state. Note that only pyrolyzed states are involved in this estimate (no bimatrix states). Thus, $\eta_{SiC,0\rightarrow i}$ is the net effect of all the impregnations/pyrolysis densification cycles.

Now at the state $i = P$ there is no matrix fraction (neglecting the rigidization coating for the moment) and the billet consists only of the dry woven preform structure whose weight is the same as the fiber weight $W_P = w_f$, which remains constant throughout. Estimates involving weight changes that occur during matrix densification typically pertain to varying matrix constituents while constant quantities tend to cancel out. Components such as the fiber weight and volume w_f and v_f do not play a role in the matrix densification process and are eliminated in the calculations, while those pertaining to the initial carbonized pitch fraction such as w_c and v_c are only relevant during the initial C-C stage and vanish beyond that . For instance, the weight gained by the dry preform billet as a result of the pitch impregnation and pyrolysis/carbonization cycle during conversion from the step $i = P$ to the first ceramic (or carbon) state at $i = 0$ is given by . . .

$$\eta_{g,P} = \frac{W_0 - W_P}{W_P} = \frac{w_c}{W_P} = \frac{w_c}{w_f}$$

where the preform substrate weight changes by $W_P = W_0\left(1+\eta_{g,P}\right)^{-1}$ and the total matrix weight fraction at $i = 0$ becomes $m_{w,0} = w_c / W_0$ . . . or . . .

(3A) $$m_{w,0} = 1 - \frac{w_f}{W_0} = 1 - \frac{w_f}{W_P\left(1+\eta_{g,P}\right)} = 1 - \left(1+\eta_{g,P}\right)^{-1}$$

At the first pyrolyzed state, the matrix consists solely of inorganic carbon deposit, so the total matrix weight and associated weight fraction (total matrix content) is just that of the carbon, respectfully . . . $w_{m,0} = w_{c,0}$ and $m_{w,0} = m_{c,0}$ (the rigidization material probably comprises less than 1% of the matrix and will be neglected here). The pitch impregnation/pyrolysis step starts the matrix densification process by coating about 17 to 19% carbonized pitch onto the pore walls and fiber surfaces of the undensified preform. But there is still much porosity to be filled with subsequent SiC densification cycles, which comprise the overwhelming majority of the densification process. The first impregnation/cure with SMP-10 polymer takes the substrate from the ceramic state $i = 0$ to the bimatrix state $i = 0B$ in which the total weight of matrix is $w_{m,0B} = w_c + w_{SiC',0}$ and the total matrix content becomes $m_{w,0B} = m_{c,0} + m_{SiC',0B}$ (where *SiC'* refers to cured but unconverted semi-organic SMP-10 polymer and *SiC* is just SiC ceramic).

The polymer impregnation (or infiltration) step is carried out on the article in a vacuum chamber in which vacuum pressure is used to force liquid SMP-10 polymer resin into the pores of the substrate. After manually removing excess resin from the surfaces of the slab, it is cured in an autoclave to crosslink and harden the polymer in place. The impregnation/cure weight gain that occurs as the substrate is taken from the $i = 0$ ceramic state to the $i = 0B$ bimatrix state is . . .

$$\eta_{g,0} = \frac{W_{0B} - W_0}{W_0} = \frac{w_{SiC',0B}}{W_0}$$

In this step, the substrate weight is changed by the amount $W_0 = W_{0B}\left(1+\eta_{g,0}\right)^{-1}$ while the original preform billet changes by $W_P = W_{0B}\left(1+\eta_{g,0}\right)^{-1}\left(1+\eta_{g,P}\right)^{-1}$. The matrix content at the bimatrix state $i = 0B$ is then . . .

$$m_{w,0B} = 1 - \frac{w_f}{W_{0B}} = 1 - \frac{w_f}{W_0\left(1+\eta_{g,0}\right)}$$

$$m_{w,0B} = m_{w,0}\left(1+\eta_{g,0}\right)^{-1}$$

or in terms of the original pitch densification weight gain . . .

$$m_{w,0B} = 1 - \left(1+\eta_{g,P}\right)^{-1}\left(1+\eta_{g,0}\right)^{-1}$$

After the $0B$ impregnation and cure, the substrate is subjected to low temperature pyrolysis which converts the crosslinked polymer matrix into amorphous silicon carbide (a-SiC). The ceramic yield y is the weight of cured pre-ceramic polymer remaining after pyrolysis, that is, $y = SiC'/SiC$, a constant which runs in the 75-85% range for SMP-10 (precise measurements of y are typically acquired by the manufacturer and/or vendor). Thus, the pyrolysis weight loss that occurs as the substrate is converted from the $0B$ bimatrix state to the second ceramic state $i = 1$ is . . .

$$\eta_{l,1} = \frac{W_{0B} - W_1}{W_{0B}} = \frac{W_{SiC',0B}\left(1-y\right)}{W_0\left(1+\eta_{g,0}\right)_0}$$

which becomes . . . $\eta_{l,1} = \eta_{g,0}\left(1-y\right)\left(1+\eta_{g,0}\right)^{-1}$

Here, the substrate weight changes by . . . $W_{0B} = W_1\left(1-\eta_{l,1}\right)^{-1}$ while the original preform weight is modified accordingly . . . $W_P = W_1\left(1-\eta_{l,1}\right)^{-1}\left(1+\eta_{g,0}\right)^{-1}\left(1+\eta_{g,P}\right)^{-1}$, and the total matrix content then becomes . . .

$$m_{w,1} = 1 - \frac{w_f}{W_0\left(1+\eta_{g,0}\right)\left(1-\eta_{l,1}\right)}$$

$$m_{w,1} = 1 - \left(1+\eta_{g,P}\right)^{-1}\left(1+\eta_{g,0}\right)^{-1}\left(1-\eta_{l,1}\right)^{-1}$$

Thus, the matrix content at each of the ceramic states can be given by . . .

at $i = 0$ . . . $m_{w,0} = 1 - \left(1+\eta_{g,P}\right)^{-1}$

at $i = 1$ . . . $m_{w,1} = 1 - \left(1+\eta_{g,P}\right)^{-1}\left(1+\eta_{g,0}\right)^{-1}\left(1-\eta_{l,1}\right)^{-1}$

at $i = 2$ . . . $m_{w,2} = 1 - \left(1+\eta_{g,P}\right)^{-1}\left(1+\eta_{g,0}\right)^{-1}\left(1-\eta_{l,1}\right)^{-1}\left(1+\eta_{g,1}\right)^{-1}\left(1-\eta_{l,2}\right)^{-1}$

. . . and so on . . .

In general . . .

(4A) $$m_{w,i} = 1 - \left(1+\eta_{g,P}\right)^{-1} \prod_{0}^{i} \left(1+\eta_{g,i-1}\right)^{-1} \left(1-\eta_{l,i}\right)^{-1}$$

which allows estimation of the total matrix weight fraction at any subsequent process state based on the original carbonized pitch weight gain in the preform billet.

All this is simply an extension of what happens to the initial dry preform weight W_P as it incrementally and sequentially progresses through the densification process to the state i . . .

$$W_P = W_0\left(1+\eta_{g,P}\right)^{-1} = W_1\left(1+\eta_{g,P}\right)^{-1}\left(1+\eta_{g,0}\right)^{-1}\left(1-\eta_{l,1}\right)^{-1} = W_i\left(1+\eta_{g,P}\right)^{-1}\prod_{0}^{i}\left(1+\eta_{g,i-1}\right)^{-1}\left(1-\eta_{l,i}\right)^{-1}$$

The cumulative ceramic weight gain from the first pyrolyzed state ($i=0$) to any future ceramic (pyrolyzed) state is a function only of the SiC ceramic gain (rather than the total matrix), accordingly . . .

$$\eta_{c,0\to i} = m_{SiC,i}\prod_{1}^{i}\left(1+\eta_{g,i-1}\right)^{-1}\left(1-\eta_{l,i}\right)^{-1}$$

A plot of $\eta_{c,0\to i}$ should parallel that of the matrix content as it progresses through the process.

Now the matrix content can be expressed in terms of the progressive state densities by recognizing that the bulk volume of the preform/substrate remains constant throughout the process (state-to-state bulk volume changes, if they occur, are infinitesimal) . . .

$$\eta_{g,(i-1)} = \frac{W_{(i-1)B} - W_{(i-1)}}{W_{(i-1)}} = \frac{\rho_{b,(i-1)B} - \rho_{b,(i-1)}}{\rho_{b,(i-1)}} \qquad \text{and} \qquad \eta_{l,i} = \frac{W_{(i-1)B} - W_i}{W_{(i-1)B}} = \frac{\rho_{b,(i-1)B} - \rho_{b,i}}{\rho_{b,(i-1)B}}$$

which means that . . $\left(1+\eta_{g,(i-1)}\right) = \rho_{b,(i-1)B} / \rho_{b,(i-1)}$ and $\left(1-\eta_{l,i}\right) = \rho_{b,i} / \rho_{b,(i-1)B}$

and finally (for ceramic states only) . . .

(5A) $$m_{w,i} = 1 - \prod_{P}^{i} \rho_{b,i-1} / \rho_{b,i}$$

Development of composite physical properties across the densification process occurs incrementally as the substrate is subjected to each PIP cycle consisting of impregnation with resin (or resin/particle slurry), autoclave cure and then 1550° pyrolysis. After the 5th and 10th cycles, the slabs are subjected to a 3000° heat treatment cycle which crystallizes the glassy SiC matrix. Composite densities, matrix content (and matrix volume) and most mechanical properties are increased substantially after the first few cycles and then gradually taper off after that. This trend is depicted in Figure 8 which shows bulk density evolution for one of the C/C-SiC slabs (the two heat treatment steps applied are indicated).

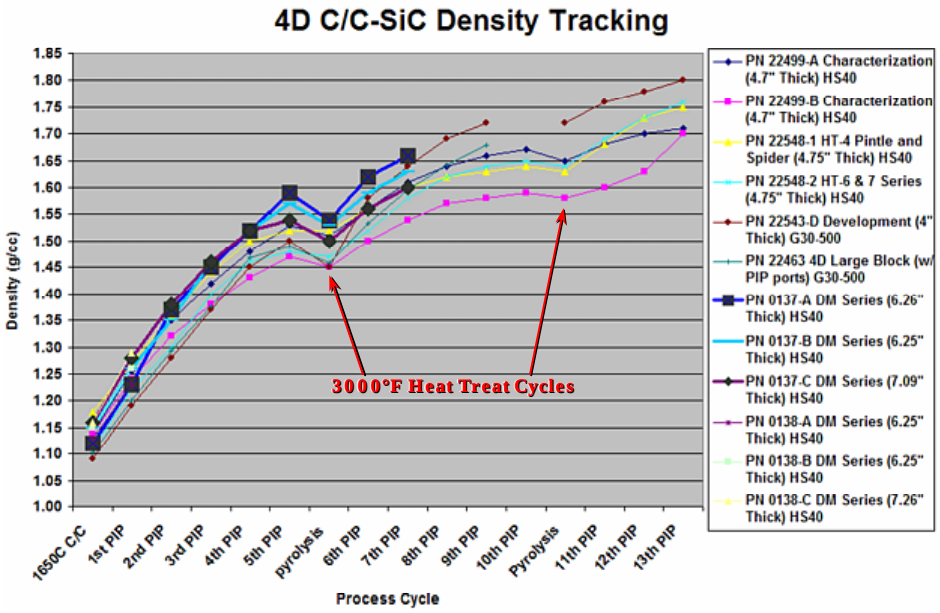

Figure 8. Cumulative increase in composite bulk density as various preform slab sections were processed through XXX's CMC densification process. Taken from the presentation, "XXX Ceramic Matrix Composite System" for the Orion LAS ACM. The current author has indicated where the HHT treatments were applied, after PIP cycles 5 and 10.

This trend is typical of CMC and C-C materials undergoing sequential densification processing. Many studies have demonstrated similar behavior for most of the critical constituent properties and some of the mechanical attributes as they progress across the densification process including composite bulk density, true density, matrix content, matrix volume, fiber content, flexural strength and interlaminar (or interlayer) tensile strength. Moreover, this behavior has been shown to exhibit a functional component and can also be defined in terms of substrate impregnation weight gains and pyrolysis weight losses[2]. Experimental validation has confirmed that functional (analytical) descriptions of these properties tend to follow exponential (response function) type characteristics asymptotically approaching their maximum (or minimum) value as they change across the densification process. Indeed, using the data given in Figure 8, unique model curves can be developed for each of the three segments of any of the slab articles . . . from the C/C state through the first 3000° heat treat after the 5th PIP, and from that point to the second heat treat after the 10th PIP, and then from there on out. Specifically, the evolution of constituent properties P for any given segment as well as over the entire densification process can be precisely tracked with a generic response function of the form . . .

$$P = A\left(1-e^{-ki}\right) + C$$

where i is the densification state (or cycle), $C = P_0$ is the initial value of the property P at $i = 0$ (the carbon state) and $A = P_{max} - P_0$, which brings clarification to the more descriptive form . . .

$$P = \left(P_\infty - P_0\right)\left(1-e^{-ki}\right) + P_0$$

Consider data specifically for the 22499-A slab section shown in Figure 8. While a more precise evaluation of the data could definitely be established by evaluating each of the three densification segments individually, pre-trials have indicated that treatment of the entire data set as one continuous densification process is sufficient for the current discussion in demonstrating the validity of this approach (more elaborate treatments of the individual segments can be pursued at a later time if necessary). Figure 9 gives a consolidated plot of the data for article 22499-A as extracted from the density data in Figure 8 along with the average model curve fit.

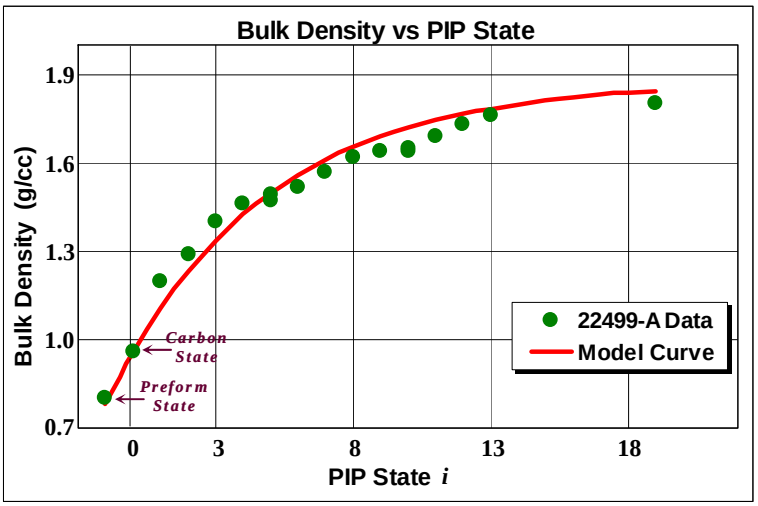

Figure 9. Plot of density data for slab section 22499-A extracted from Figure 8 with overlay of the average model curve fit.

For the 22499-A slab, the final (average) bulk density is known to be 1.80 g/cc, that of the dry preform was 0.8 g/cc, and 0.96 g/cc after the pitch carbon densification step. The functional description for the bulk density of the 22499-A slab based on this data was determined to be best represented by . . .

$$\rho_b \cong 0.92\left(1 - e^{0.18i}\right) + 0.96$$

where $\rho_{b,0} = 0.96$ g/cc is the bulk density of the slab after pyrolysis of the mesophase pitch fraction and ρ_b approaches an average of . . . $0.92 + 0.96 \cong 1.88$ g/cc after an infinite number of SiC densification cycles (if that were possible).

Now the density of HS40 (PAN) fiber is given as 1.85 g/cc and since $\rho_b = f_v\rho_f + m_v\rho_m$ the initial fiber volume fraction of the dry (undensified) preform can be estimated. Recall this structure has not yet received any densification treatments and thus contains zero matrix (other than the rigidization coating which is unknown at this point but presumed to be insignificant for this analysis). Using the dry preform bulk density of 0.8 g/cc, the fiber volume fraction comes out to be . . .

$$f_{v,P} = \rho_b / \rho_f = 43.24\%$$

It is safe to assume this value does not measurably change throughout the entire densification process and so the original fiber volume fraction is the same as the final fiber volume. Now the matrix weight fraction is also given by . . . $m_w = 1 - f_v\rho_f / \rho_b$, whose only variable (in this particular relation) is the composite bulk density. A plot of the matrix content (as a function of the bulk density data from Figure 8) is given in Figure 10 below along with its model curve which, as with the bulk density functional fit, is intended to be representative of the matrix content across the entire spectrum.

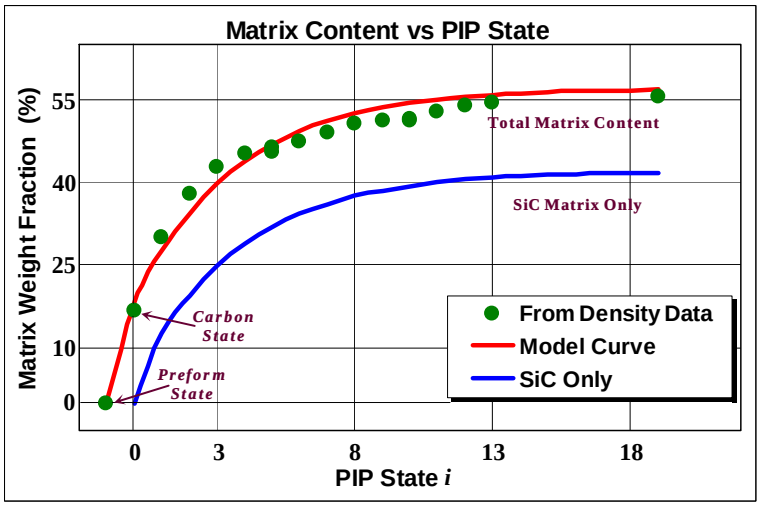

Figure 10. Plot of the matrix content based on bulk density data for slab section 22499-A with overlay of the average model curve fit.

This analysis implies an carbon matrix weight fraction in the range 17-19% deposited from the initial pitch densification step which remains unchanged from that point on. Matrix fractions in these kinds of composites are extremely difficult to physically measure and so an estimation technique such as this can sometimes prove beneficial during design and characterization processes. Now the average functional description for the Total Matrix Content in the 22499-A slab was determined to be . . .

$$m_w \cong 38.6\left(1 - e^{0.27i}\right) + 18.5$$

where $m_{w,0} \cong 18.5\%$ is the carbon matrix content after pyrolysis of the mesophase pitch fraction and the total m_w approaches 57.1% after an infinite number of SiC densification cycles (if that were possible). A similar scenario could be developed for the SiC portion of the matrix which tops out at around 41-42%.

Now as the substrate density increases over the process, the open porosity decreases as it gradually becomes occupied with matrix material. While other properties are represented by increasing functions, the porosity decreases in an inverse manner. Evolution of the porosity volume fraction can be explored in a likewise manner by applying the following formula . . .

$$p = 1 - f_v - m_w \rho_b \rho_m^{-1}$$

However, the matrix density is a complex combination of the carbonized pitch, crystalline (β) SiC and amorphous SiC (these two SiC densities are *not* identical), but a rough estimate can be surmised by making note of the various fractions for each matrix component and the approximate densities. Green (amorphous) coke has a density of about 1.3 (far from the crystalline order of pure graphite whose x-ray density is 2.25); for this case, the density of crystalline β-SiC is taken as 3.0 (pure electronic grade β-SiC has an x-ray density of 3.22, but the SiC in these articles is known to contain carbon as well as other impurities and defects); amorphous SiC (especially the form derived from SMP-10) has been reported to have a density of about 2.4[1]. Using Figure 2 as a reference, the matrix fraction is considered to be comprised of about 17% a-C, 58% β-SiC and 25% a-SiC, which gives an approximate composite matrix density of about . . .

$$\rho_m = \left(0.17\rho_{a\text{-}C}^{-1} + 0.58\rho_{\beta\text{-}SiC}^{-1} + .25\rho_{a\text{-}SiC}^{-1}\right)^{-1} = 2.33 \text{ g/cc}$$

A plot of the 22499-A open porosity throughout the densification process (as a function of the original bulk density data from Figure 8) is given in Figure 11 along with the model function representing the open porosity of the substrate across the entire densification domain and beyond.

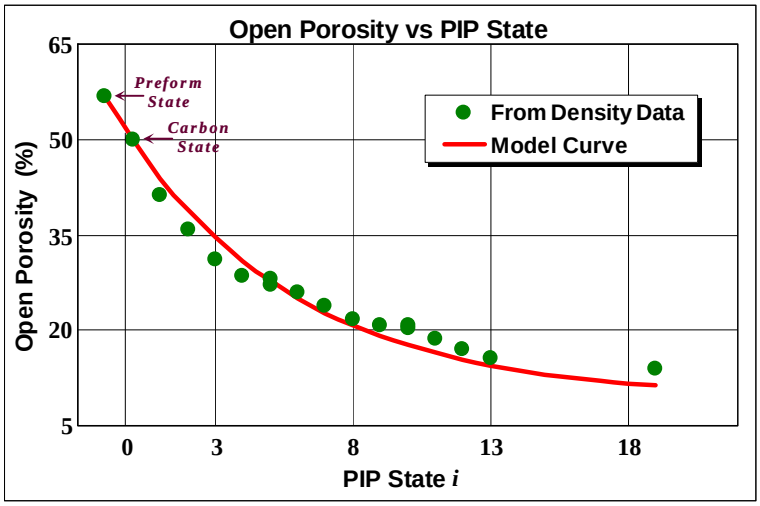

Figure 11. Plot of the open porosity based on bulk density data for slab section 22499-A with overlay of the average model curve fit.

[1] Information acquired from independent or undisclosed sources.

Behavior of the porosity fraction is almost the exact converse of that for the bulk density because as the SiC matrix fills the porosity, the bulk density increases accordingly. The optimized functional description for the open porosity of the 22499-A slab as it progresses through the densification process has been determined to be . . .

$$p \cong 40.6\, e^{0.16i} + 9.3$$

The initial porosity of the dry woven preform is simply $1 - f_v = 56.8\%$. After the pitch densification cycle, the slab/substrate porosity is estimated to be $p_0 = 40.6 + 9.3 = 49.9\%$, and after unlimited densification cycles (if it were possible), the porosity would approach an average of $p_\infty = 9.3\%$.

The true or real density of a composite is the density of the non-pervious portion of the material, that is . . . $\rho_t = \rho_b / (1 - p)$. It is the bulk density less the influence of the porosity fraction, or the combined density of just the fiber and matrix. It is always higher than the bulk density. Relationships between these densities and the open porosity for the 22499-A slab are illustrated in Figure 12.

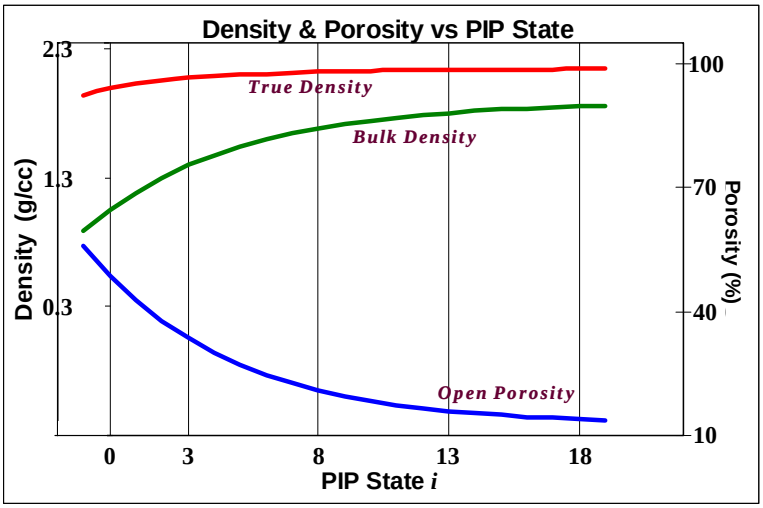

Figure 12. Model curves for the bulk density, true density and open porosity for the.22499-A slab.

True density is sometimes a measure of fiber-to-matrix binding and has been shown to heavily influence mechanical attributes in such tests as flexural, interlayer shear, interlayer tensile, longitudinal compression and differential CTE (in the longitudinal direction). Since the bulk density includes the porosity fraction, it will tend to have a attenuating effect on mechanical and thermal conduction as well as shock propagation and vibrational damping. However, it will also affect (negatively) the same properties given above because higher levels of pores and voids will reduce fiber-to-matrix contact area.

Now an expression defining the evolution of the matrix content across the ceramic densification process can be derived in terms of the impregnation weight gains and pyrolysis weight losses. However, XXX holds the records for this data. In lieu of the slab weight changes, matrix content estimation can be formulated in terms of state-to-state substrate densities using the data depicted in XXX's chart of Figure 8 and Eq(5A) developed in the Appendix (see the Appendix for derivation of all expressions, nomenclature and notation used in this discussion). With this simplified formula, the total matrix content m_w can be computed for each of the ceramic states i throughout the process starting with the dry preform state P and progressing across all the subsequent states, $i = 0,1,2,3,...$

$$m_{w,i} = 1 - \prod_{P}^{i} \rho_{b,i-1} / \rho_{b,i}$$

As expected, the set of values derived from this expression are an exact match for the plotted values and the model curve already produced in Figure 10 for the total matrix content. This approach opens the door to precise characterizations of all the other material constituents based solely on measured bulk densities (or impregnation/pyrolysis weight changes). Constitutive representations for matrix volume fraction,

fiber weight fraction, ceramic weight gain, matrix density, flexural strength and interlayer strength are sometimes only vague perceptions the manufacturer/designer wishes they had a better hold on.

It might be noted that all of the preceding results developed in this discussion represent average, overall properties for the entire slab, and it should be realized . . . each property will inevitably vary from one point in the substrate body to the next. Both 2-D and 3-D composites are highly anisotropic, non-homogeneous materials. By their very nature, the non-uniformity and anisotropy characteristics of composite materials are not only inherent by design, but are also governed by a host of manufacturing parameters and process conditions which influence the distribution of material properties throughout the body, and many of these variables are beyond the manufacturer's control (unfortunately). Thus, this analysis cannot necessarily detect nor fully address the spot-to-spot variability that likely played a role, to some degree, in the recent HT-5 and HT-7 failures.

If preceding analysis were broken down further and a more detailed evaluation was performed to account for the two 3000° heat treat steps, all of the previous values and functional results given above would shift (slightly). As a matter of fact, if additional heat treat cycles were applied to the material across the process, more of the open porosity could be densified and reduced perhaps down close to the 3-5% level, but the exact ramifications of this porosity level on the performance properties of the final product in the ACM application cannot be ascertained at this time. It should be realized that since each pyrolysis creates new pores and voids, a final porosity of zero is impossible – the bulk density will never reach the true density and the two will never coincide.

It should also be noted here that the final average porosity of ~13% as reported by XXX for these articles is not the total porosity fraction of the composite but pertains to the 'open' porosity, that is, the fraction of pores, voids and cavities that are accessible to intruding fluids. The porosity and densities values given in Figures 7 and 8 were measured by an Archimedes-type technique using water or solvent which generates an apparent or 'open' porosity fraction and associated bulk density. The apparent 'true' composite density is estimated from these values and, most importantly, the level of 'closed' or sealed porosity is completely unknown. What is known however, is that the inaccessible fraction of the total porosity fraction for these types of 3-D composites can be quite substantial, sometimes double the level of the measurable open porosity.

Selected excerpts taken from **"Density, Porosity & Constituent Fractions in C-C/SiC"**, *Randy Lee*

Bulk Density: Functional Characterization & Estimations

It is obvious from Figure 1 that the greatest weight gains occur in the first few cycles which gradually taper off after many cycles have been completed. Independent studies have established that this behavior can be tracked along a generalized response function of the type . . .

$$P = A\left(1 - e^{-ki}\right) + C$$

or specifically for the C-C/SiC bulk density . . .

$$\rho_{b,i} = \left(\rho_{b,\infty} - \rho_{b,0}\right)\left(1 - e^{-ki}\right) + \rho_{b,0}$$

where $\rho_{b,i}$ is the composite bulk density at any given pyrolyzed state *i* along the densification path; $\rho_{b,\infty}$ is the bulk density after an infinite number of densification cycles (if that were possible); and $\rho_{b,0}$ is the bulk density at the beginning of the ceramic densification process, after the C-C matrix phase has been incorporated into the substrate. Thus, while the weight gains become smaller and smaller, the incremental (step-by-step) increases in bulk density also become smaller . . . as the bulk density asymptotically approaches a hypothetical maximum or threshold density at $\rho_{b,\infty}$.

Over the last year or so, much of the information needed to roughly define the XXX C-C/SiC material system and manufacturing process has eventually become available but early on, a couple of pieces of critical data were necessary to effectively construct a comprehensive picture of the densification process and the associated physical property response characteristics. During one-on-one communications with XXX personnel following the HT-5 test fire, approximate values were obtained independently (and discreetly) for the average bulk density of the freshly woven preform structure . . . $\rho_{b,-2}$ = ~ 0.81 g/cc, and the average bulk density after pyrolysis of the rigidized preform . . . $\rho_{b,-1}$ = ~ 0.96 g/cc. Note that the density tracking data given in Figure 1 above is a composite plot depicting multiple densification runs performed by XXX on various billets, slabs and test articles during their development work for the C-C-SiC product concept. This data is re-plotted in Figure 2 below, less the two 3000° HT states, but including the two additional density states ($\rho_{b,-2}$ and $\rho_{b,-1}$) and a precisely modeled curve fit. The resulting model functional expression also follows . . .

Figure 2. Re-plot of the data in Figure 1 along with a precise model fit and two new points of interest.

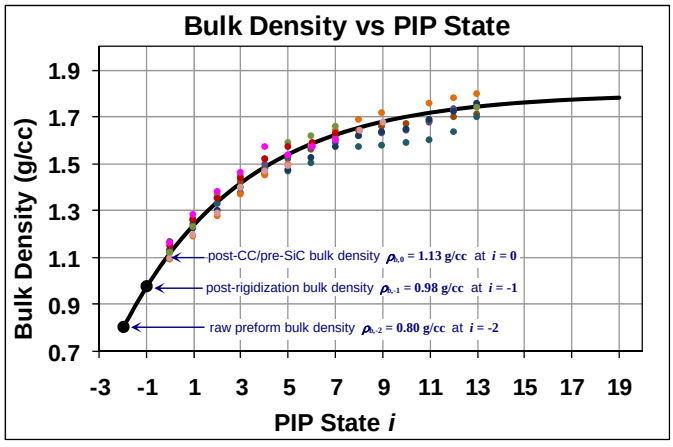

$$\rho_{b,i} = 0.68\left(1 - e^{-0.2i}\right) + 1.13$$

Here, the bulk density at the C/C state (i = 0) is given as $\rho_{b,0}$ = 1.13 g/cc (in good agreement with the value in Table 2) and the bulk density at infinite densification (if that were possible) is estimated simply as $\rho_{b,\infty}$ = 0.68 + 1.13 = 1.81 g/cc. Values are tabulated for selected model states in Table 3 below. It is obvious the model predictions are in good agreement with known values . . .

Table 3. Selected points of interest along the C-C/SiC bulk density model curve.

Dry Preform State i = -2	Rigidization State i = -1	Carbon Pitch State i = 0	1st Ceramic State i = 1	5th Ceramic State i = 5	10th Ceramic State i = 10	13th Ceramic State i = 13	∞th Ceramic State i = ∞
0.80 g/cc	0.98 g/cc	1.13 g/cc	1.25 g/cc	1.56 g/cc	1.72 g/cc	1.76 g/cc	1.81 g/cc

Note that $\rho_{b,\infty}$ = 1.81 g/cc at $i = \infty$ is projected to be the average maximum bulk density achievable for this material system under the particular fabrication conditions applied and raw materials incorporated (relative to the *open* porosity, of course). This bulk density upper limit is accompanied by a corresponding average minimum limit for the open porosity and an average maximum limit for the true density. Both of these parameters will also be developed shortly. It should be emphasized here that this is the *average* maximum bulk density with respect to the collective series of data curves contained in Figure 1 – individual slabs and articles will exhibit higher or lower curves giving threshold bulk densities that can range anywhere from about 1.70 to 1.85 g/cc.

It should be realized that each densification cycle associated with essentially all PIP-type process approaches accomplishes two effects . . . (1) Permeation and densification of open, accessible pores and cavities, and (2) Closing and sealing of pore tunnels and narrow interconnects leading to larger cavities which were formerly accessible. Unfortunately, a certain level of pores are closed off during each densification cycle. The partial fractions of open and closed porosity vary from cycle to cycle and there are indications that the fraction of trapped pores increases with each cycle. Thus, the surmised true density at any given state must contain this 'error', and as long as closed pores and voids are created with each cycle, the bulk density will never come close to the true density.

Immediately after dry weaving, the preform must be rigidized in order to prevent deformation or damage to the fibers which can be imparted during handling and subsequent processing. There is not enough information available to fully substantiate the exact rigidization process XXX utilized on the freshly woven preform structure. However, examination of some of the photos provided strongly suggests that rigidization was accomplished by restraining the billet preform in a specially fabricated cage assembly using a low viscosity liquid thermoset polymer which was allowed to passively soak into the preform structure and harden (crosslink) at room temperature. A number of polymer types could be used for this purpose where the preform structure is essentially casted in an opaque plastic and then carbonized to yield a thick glassy carbon fiber coating which appears to constitute a significant portion of the total carbon matrix fraction. Pyrolysis of the casted preform containing these types of thermoset polymers would only yield a small char residue but would leave a very open (and rigidized) porous structure for safe pitch resin impregnation. This initial carbon deposit will permanently remain in the glassy state since glassy carbon forms are non-graphitizing structures.

After rigidization of the preform, pitch densification can then be carried out using more aggressive processing/handling techniques including high temperature, vacuum and pressure and physical manipulation with heavy duty cranes and fixturing hardware. Following rigidization and pyrolysis, XXX indicates that a single pitch impregnation/pyrolysis cycle is applied (their so called 'low graph 3000°F cycle), which insures that the carbonized pitch fraction is left in an amorphous hardened mesophase state (4000°-4500°F would easily graphitize this carbon form but the C-C/SiC material never sees that temperature). Thus, the carbonaceous phase in XXX's C-C/SiC system appears to be comprised of two sub phases (or partial fractions) . . . glassy carbonized rigidization polymer followed by carbonized mesophase pitch. Other than the 2-D graphene layers comprising these two carbon forms, this phase contains no 3-D crystallites and is pseudo-amorphous throughout.

For both 2-D and 3-D type composite structures, geometrical volume changes after the rigidization or laminate molding process have been documented to be infinitesimal or immeasurable throughout the densification process. For 2-D laminated systems, volume shrinkages on the order of 2% in the thickness direction may occur during the first pyrolysis cycle going from the molded state to the first C/C state. Beyond this cycle however, volume changes are immeasurable, infinitesimal or nonexistent. For 3-D composite systems, in particular the XXX C-C/SiC system, the weaving process establishes all three dimensional boundaries and unit cell parameters of the preform structure at the onset and then the rigidization process permanently fixes these attributes in space.

Thus, it should be recognized that the fiber volume fraction (or 'fiber volume') of all C-C/SiC articles is permanently established in the billet state before any densification cycles are ever applied and it remains invariant from that point on (only changing slightly after the coating phase is applied). As such, the Table 2 value of $f_v = 43.6\%$ is considered to be the constant average fiber volume fraction of C-C/SiC articles . . . since *the substrate volume remains constant throughout the entire process*, so does the fiber volume. However, the fiber *weight* fraction f_w is not constant because it gradually increases over the process in accordance with the decreasing matrix weight fraction m_w, a fact that is exemplified by the rule [1] . . . $f_w + m_w = 1$. This helps to facilitate the understanding that substrate densification is most appropriately defined as *matrix densification*.

For the C-C/SiC system, the fiber volume can be directly estimated before any processing begins by obtaining accurate measurements for the dry billet (preform) weight W_{-2} and corresponding geometrical volume V (the constant substrate volume $V = V_{-2} = V_{-1} = V_0 = V_1 = V_2 = etc...$). If measurements are carefully taken (as XXX has apparently done), the bulk density in the dry preform state $i = -2$ can be determined. On the average, this turns out to be $\rho_{b,-2} = 0.81$ g/cc (from Table 3). In this process state, the HS40 fibrous preform is the only weight constituent present, that is, $f_{w,-2} = 1$, and so the fiber volume is estimated [1] simply by using Mitsubishi's measured (average) fiber density $\rho_f = 1.85$ g/cc (from Table 1) and the bulk density of the dry preform structure, that is . . .

$$f_v = f_{w,-2}\frac{\rho_{b,-2}}{\rho_f} = 1 \times \frac{0.81\ \text{g/cc}}{1.85\ \text{g/cc}} \approx 43.6\%$$

For organic-based PMC systems, the resin content (matrix weight fraction) at the molded (post-autoclave) state can be directly measured using such robust tests as ASTM nitric acid digestion, but this technique is ineffective for pre-ceramic (semi-organic) polymers. Thus, from this point on, quantities such as matrix content, matrix volume and matrix density must be obtained indirectly by estimations based on weights and geometrical dimensions (for the current study at hand, the bulk density values given in Figure 1 are the only data available for this purpose). Partial matrix fractions and the composite matrix density are complex, requiring even more intricate estimation techniques to yield useful and productive values (as covered in Appendix IV and V). It goes without saying, any meaningful analysis in this regard is entirely at the mercy of the good techniques practiced by the floor engineers and technicians responsible for precisely measuring these raw parameters.

A more robust approach would include both of the 3000° heat treat steps after PIP cycles 5 and 10. This would call for a more complex characterization of the data in multiple segments rather than a single function, but it would improve tracking accuracy along with more precise projections near the extremes. For demonstration purposes, omitting these two HT states does not introduce enough error to substantially affect the results. However, as will be seen shortly, effective characterization of the porosity here will require at least an elementary estimation of the partial matrix fractions and the complex matrix density from which the 3000° HT points will be taken into account.

Matrix Content: Functional Characterization & Estimations

The raw bulk density values provided in Figure 1 can be used for estimation of other constituent quantities relevant to the C-C/SiC system as it undergoes densification processing. For instance, using equations represented in Appendix II or Eq(5B) in Appendix V, the total matrix content m_w at any densification state i can be estimated directly from the corresponding bulk density value at the same state $\rho_{b,i}$, that is . . .

$$m_{w,i} = 1 - f_v \rho_f \rho_{b,i}^{-1} \qquad \text{or} \qquad m_{w,i} = \left[1 + \rho_{b,-2}\left(\rho_{b,i} - \rho_{b,-2}\right)^{-1}\right]^{-1}$$

Figure 3 gives a plot of data generated from either of these formulas directly from the measured bulk densities along with a precise model fit best describing its behavior.

Figure 3. Total matrix content and model fit across the process estimated directly from the bulk density data in Figure 2.

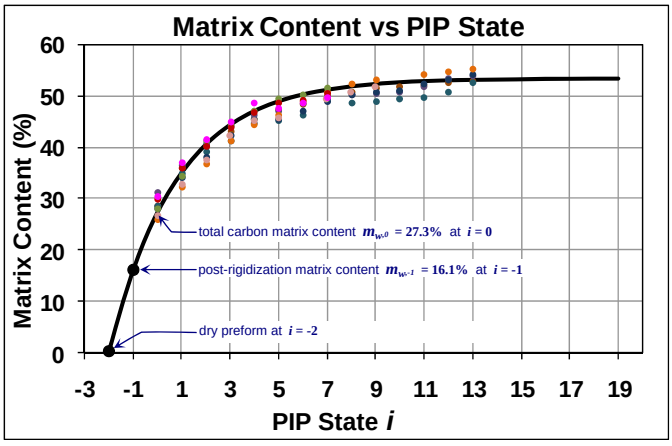

$$m_{w,i} = 26.2\left(1 - e^{-0.354i}\right) + 27.3$$

At the state $i = 0$, the matrix contains only inorganic carbon and its content is estimated to be $m_{w,0}$ = 27.3%. As with the bulk density model, the total matrix content after an infinite number of densification cycles (the threshold matrix content) is given simply as $m_{w,\infty}$ = 26.2 + 27.3 = 53.5%. Model values are tabulated for selected states in Table 4 below . . .

Table 4. Selected points of interest along the C-C/SiC total matrix content model curve.

Total Matrix Content

Rigidization State i = -1	Carbon Pitch State i = 0	1st Ceramic State i = 1	5th Ceramic State i = 5	10th Ceramic State i = 10	13th Ceramic State i = 13	∞th Ceramic State i = ∞
16.1 %	27.3 %	35.1 %	49.0 %	52.7 %	53.2 %	53.5 %

Here, $m_{w,\infty}$ = 53.5% is projected to be the average maximum total matrix content achievable for this material system under the particular fabrication conditions and raw materials incorporated. Again, this is the *average* maximum matrix content with respect to the collective series of data curves given in Figure 3 – individual slabs and articles will exhibit higher or lower curves giving maximum total matrix contents that can range anywhere from about 50 to 57%.

At any state during the densification process, the total matrix content is the sum of partial fractions comprising a 'quadmatrix' consisting of varying amounts of: (1) carbonized rigidization polymer (glassy carbon), (2) carbonized mesophase resin (amorphous carbon), (3) amorphous/glassy silicon carbide (a-SiC), and (4) crystallized cubic silicon carbide (β-SiC). The combination of fractions (1) and (2) make up the total carbon content while the combination of (3) and (4) comprise the total SiC portion of the total 'bimatrix'. Comprehensive estimations for the partial matrix fractions in the C-C/SiC system and the technique used are given in Appendix IV. The graphical and tabulated results provided in Appendix IV reveal an interesting distribution for each of the four co-constituents comprising the total matrix phase within the C-C/SiC system. Results for selected states calculated from the bimatrix model in Appendix IV are given in Table 5 below . . .

Table 5. Selected points of interest along the C-C/SiC bimatrix content model curve given in Appendix IV.

Bimatrix Content

	Carbon Pitch State i = 0	1st Ceramic State i = 1	5th Ceramic State i = 5	10th Ceramic State i = 10	13th Ceramic State i = 13	∞th Ceramic State i = ∞
Total C	28.3 %	25.3 %	18.8 %	16.3 %	15.8 %	15.4 %
Total SiC	0.0 %	9.3 %	28.7 %	36.0 %	37.3 %	38.4 %

Values determined from this approach (Appendix IV) are in fair agreement with those provided by the total matrix content model developed above in Table 4 (recall the total matrix content at any state is simply the sum of the carbon and SiC fractions at that state; the C fractional content gradually decreases as the SiC content increases across the process). Incidentally, the bimatrix model projection implies that the total carbon content at the end of the process and beyond is about 15-16% while the total SiC content never completely reaches the 40% level.

The corresponding open porosity fraction p_o at any state i can also be estimated directly from the raw density values given in Figure 1 by using Eq(7A) or (8A) developed in previous sections,

(8A) $$p_{o,i} = 1 - \rho_{b,i}\rho_{m,i}^{-1} - f_v\left(1 - \rho_f \rho_{m,i}^{-1}\right)$$

However, before these estimations can be carried out, corresponding values for the *matrix density* must be determined. For the C-C/SiC system, the matrix density is physically complex since it consists of four co-constituents each of which vary from state to state. It is a composite density in which a functional bulk density for each matrix co-constituent must be ascertained. This is difficult because 'bulk' densities are automatically dependent on the particular materials, processes and conditions to which the parameter is associated or measured. The constituent bulk densities given earlier in Table 1 were presented with emphasis to the C-C/SiC and like systems. Generalized bulk density can be ambiguous since its volume boundaries are often specified by the test methods used to define a given system (i.e... pour density, tap density, foam density, apparent density, etc . . .).

Before the incremental composite matrix densities can be determined however, the distribution of partial matrix fractions for each of the co-constituents must be developed. The techniques used to estimate partial matrix weight fractions and the composite matrix densities are given in Appendices IV and V respectively, along with their results [1]. Table 5 above presented a small portion of this analysis. All that will not be rehashed here. Rather, with representative estimates for the matrix density at hand, the open porosity fraction for the C-C/SiC system can be evaluated similarly to the functional descriptions for substrate bulk density and the total matrix content developed above. Using the raw density values given in Figure 1 and the formula above, a corresponding plot and model curve for the open substrate porosity fraction are given in Figure 4 below followed by the representative response function which best describes its behavior . . .

Figure 4. Open porosity fraction and model fit across the process estimated directly from the bulk density data in Figure 2.

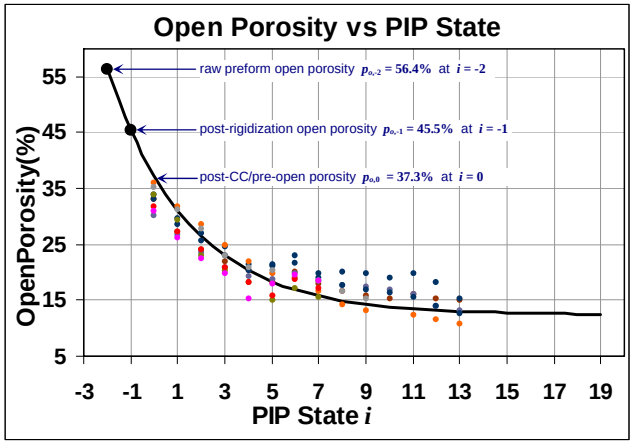

$$p_{o,i} = 24.9\, e^{-0.285i} + 12.4$$

[1] Please consult Appendices B and C for a description of the methodology used to estimate partial matrix fractions and the complex matrix density.

At the state $i = 0$, the open porosity fraction is indicated to be $p_{o,0} = 21.8 + 13.1 = 37.3\%$, while its value after infinite densification (if that were possible) is simply $p_{o,\infty} = 12.4\%$. Model estimates for selected states are tabulated below in Table 6. Results for the states $i = -2$ and $i = 13$ are in excellent agreement with measured values.

Table 6. Selected points of interest along the C-C/SiC open porosity model curve.

Open Porosity

Dry Preform State $i = -2$	Rigidization State $i = -1$	Carbon Pitch State $i = 0$	1st Ceramic State $i = 1$	5th Ceramic State $i = 5$	10th Ceramic State $i = 10$	13th Ceramic State $i = 13$	∞th Ceramic State $i = \infty$
56.4 %	45.5 %	37.3 %	31.1 %	18.4 %	13.8 %	13.0 %	12.4 %

Here, $p_{o,\infty} = 12.4\%$ is projected as the average minimum open porosity achievable for this material system under the particular fabrication conditions and raw materials incorporated. Note that in the dry preform state (at $i = -2$), before densification processing begins, the pre-determined fiber volume fraction $f_v = 43.6\%$ implies an initial open substrate porosity of $p_{o,-2} = 56.4\%$. Also note that at the end of densification (at $i = 13$), approximate open porosity values for the C-C/SiC material were previously documented by XXX/XXX engineers to be around ~13%. Both of these correlations serve to strengthen the validity of these models. Again, bear in mind that $p_{o,\infty}$ is the *average* minimum open porosity with respect to the collective series of data curves given in Figure 4 – individual slabs and articles will exhibit higher or lower curves resulting in minimum (threshold) open porosity fractions that can range anywhere from about 9 to 17%.

For liquid-densified (PIP-densified) C/C and CMC systems, the threshold porosity can never be taken to zero . . . there will always be some residual open porosity in the substrate after each densification cycle. This is because each cycle ends with a pyrolysis step which creates new pores, voids and cavities due to the expulsion of pyrolysis volatiles in combination with substantial volumetric shrinkage of the matrix material as it undergoes thermal conversion. For SMP-densified systems, this corresponds roughly to about 20% loss in polymer during pyrolysis and a 50% shrinkage of the remaining matrix during conversion into ceramic. For the current C-C/SiC system under study, this leads to a threshold porosity that approaches the ~12% level. In addition to the open (liquid-permeable) porosity, the density-porosity relationship includes a distinctive bulk (liquid-permeable) density and an associated 'true' density which pertains to the liquid-impermeable or impervious portion of the material as defined by . . . $\rho_b = (1 - p_o)\rho_t$.

In all systems of this type, the total porosity gradually decreases with each densification cycle but changes in the open and closed porosity fractions are not necessarily equivalent. There are some indications that the partial fraction of closed pores actually increases from state-to-state at the expense of the open porosity. This 'error' is inevitably built into the actual values obtained during physical measurements of bulk density and open porosity. Additionally, it is all but certain that reported FMI density/porosity values for their 3-D C-C/SiC material were determined using one of the Archimedes techniques on cubic-shaped test samples in which all six sides were machined to form the sample. This permits all six faces to reflect approximately the same inner pore structure which, because of the machining effects, exposes a mixture of both open and closed pores. In contrast, test samples extracted from 2-D composite laminates or panels usually consist of four exposed cross-sectional edges

representative of the panel thickness (in-plane), and two larger faces (the processed mold side and bag side surfaces), which are partially sealed and less pervious than the cross-sections. The errors reflected in these two sample configurations should not be discounted.

In any case, the continuation of additional densification cycles at the high end of the curve in efforts to try and fill up the last few percentages of open porosity is not cost-effective because a point of diminishing returns is reached far below the theoretical threshold porosity. However, it might be interesting to consider some of the benefits or effects that a 14th cycle might have using alternative densification techniques or matrix materials. For instance, chemical vapor deposition/infiltration (CVD/CVI) is carried out by 'cracking' gaseous reactants in a hot, evacuated chamber containing the porous article, but its ability to penetrate the deepest pores is highly sensitive to the process conditions utilized (pressure, reactant composition, temperature, residence time). CVD/CVI is commonly used to deposit polycrystalline β-SiC and quasi-amorphous pyrolytic carbon during densification and coating operations. While this method is effective at densifying the outer most micro- and meso-pores, many of the large pores and voids, such as those at the fiber bundle intersections are difficult to fill up. Additionally, CVD/CVI deposits have a tendency to accumulate faster around the pore openings and edges, often completely closing off pore tunnels leading to the interior. Both of these effects result in higher (and undesirable) levels of closed porosity. While CVD techniques have a long history throughout the C-C/CMC industry, densification of fibrous composites via forced-flow isothermal CVD/CVI has been utilized extensively in recent years, offering slightly improved deposition/infiltration effects which typically reach threshold porosities that can range anywhere from about 8% to 15% (not all too different than the current C-C/SiC system under study).

Techniques for deposition of glassy carbons via liquid (polymer) impregnation and pyrolysis (PIP) using resole-type *phenolic* resins (similar to the rigidization process discussed earlier) also have a long history, including the archaic but highly successful RCC/ACC systems. This practice uses the same approach as XXX's PIP process for their C-C/SiC material except pyrolytic volume losses for cured phenolic polymer are not nearly as high as that for SMP-10. That is, fewer densification cycles are required to reach the appropriate density level (and corresponding mechanical strengths), and the threshold porosity is lower . . . threshold porosities for phenolic-densified 3-D PAN-based C/C systems have been independently determined to be in the 7-9% range and are primarily due to large voids at the fiber bundle intersections. Unfortunately, PIP-type densification methods also have a tendency to block off pores – but to a lesser degree than most CVI/CVD approaches.

It is a matter of curiosity to wonder what the bulk density of the substrate might be if the remaining ~13% porosity in the C-C/SiC material at i = 13 was occupied with material deposited by alternative densification techniques. Of course, this would carry the substrate to the state i = 14. Appendix D includes the method for developing a simplified formula, Eq(2D) [1], which can provide estimates of this type, namely . . .

(2D) $$\rho_{b,i} = \rho_{b,o} + \left(x_v - p_t\right)\rho_x$$

[1] Please consult Appendix D for further explanations of the techniques and formulas used to estimate these hypothetical cases.

Here, $\rho_{b,\mathrm{i}}$ is equivalent to the new or final composite bulk density $\rho_{b,14}$; $\rho_{b,\mathrm{o}}$ represents the former density $\rho_{b,13}$ whose value can be taken as 1.74 g/cc from Table 2; x_v is the volume fraction of the newly added matrix material while ρ_x is its bulk density; and p_t is the threshold porosity indigenous to a hypothetical composite densified with the new material under consideration. Using Eq(2D), Table 7 below contains several scenarios of interest for matrix media and densification (application) methods which might be utilized to carry the porous C-C/SiC substrate from the i = 13 state to i = 14. Estimates for an organic solvent, ordinary water and a cured polymer resin (analogous to a Polymer Matrix Composite) are also given and provide an interesting comparisons for reference. As inferred by the results, the threshold porosity p_t has a very significant effect on the final composite bulk density $\rho_{b,\mathrm{i}}$ in spite of the density exhibited by the new matrix material ρ_x. Justifications immediately follow Table 7 supporting the various ρ_x and p_t values utilized in these simulations . . .

Table 7. Final bulk composite densities expected for various scenarios with an added densification step from i = 13 to i = 14.

Densification from the state i = 13 to the state i = 14

New Material	**Glassy Carbon**	**Pitch Carbon**	**Pyro Carbon**	**β-SiC**	**Kerosene**	**Water**	**Cured Phenolic**
$\rho_{b,x}$ of Material	1.45 g/cc [1,5]	1.35 g/cc [2]	2.05 g/cc [3]	3.2 g/cc [4]	0.817 g/cc 77°F	0.998 g/cc 77°F	1.24 g/cc [5]
App Method	PIP	PIP	CVI	CVI	wet impreg	wet impreg	impreg/cured
Threshold p_t	p_t ~ 8% [6]	p_t ~ 10% [7]	p_t ~ 12% [8]	p_t ~ 12% [8]	p_t ~ 0%	p_t ~ 0%	p_t ~ 4% [9]
Final Composite ρ_b	1.82 g/cc	1.79 g/cc	1.77 g/cc	1.78 g/cc	1.85 g/cc	1.87 g/cc	1.86 g/cc

1 - As provided in Table 1, the liquid-permeable density of glassy carbon is about the same for all polymer thermoset precursors, including rigidization polymer, cured phenolic resin, epoxies, etc . . .

2 - As provided in Table 1, the liquid-permeable density of amorphous pitch carbon which has not been graphitized is reflective of analogous bulk densities for green coke and hardened mesophase.

3 - The gas-permeable density of CVD-deposited carbon has been determined independently and by other industry sources [1]; its deposits may consist of mono/polycrystalline mixtures.

4 - The gas-permeable density of CVD-deposited SiC has been determined independently and by other industry sources[2]; on carbon substrates, its deposits are polycrystalline.

5 - Liquid-permeable densities for cured and charred phenolic resins have been extensively characterized independently (principally Borden brand resoles and novolacs, including SC-1008HS and associated and family types).

6 - The sectioned porosity threshold for phenolic-densified 3-D PAN-based C/C systems has been independently determined to be in the 7-9% range and is primarily due to large voids at the fiber bundle intersections.

7 - It has inferred from industry workers and researchers that the sectioned porosity threshold for pitch densified 3-D PAN-based C/C articles runs in the 10-12% range [3].

8 - It has been inferred from industry workers and researchers that sectioned threshold porosity values for pyrolytic and CVI-densified materials runs in the range 8 to 18%; much of the porosity consists of closed pores and larger voids at the fiber bundle intersections which are difficult to fill using CVD/CVI approaches.

9 - When impregnated effectively, liquids will occupy 100% the open porosity of a system (this includes liquid polymer resins prior to cure). Unlike many other resins, phenolics crosslink via condensation which expels water molecules and curing volatiles. When cured properly, this leads to a unique, interconnected micro-porosity network within the phenolic phase which is almost undetectable. In a composite system however, resin/matrix shrinkage during the curing process will create larger voids and pore channels along and parallel to the fiber bundles. The threshold porosity for loosely compacted composite structures (such as those derived from 3-D preforms) has been determined independently to be around 3-5% (open threshold porosities for well compacted 2-D laminates can be as low as ~1.5%).

[1] As taken from the product data sheet for Carbograf 400 pyrolytic CVD graphite and supplemented by independent testing at Poco Graphite Inc.
[2] As taken from the product data sheet for Carbosil 100 CVD SiC coating and supplemented by independent testing at Poco Graphite Inc.
[3] "Mesophase Pitch for Low Pressure Carbon/Carbon Composite Processing", Mickael Dumont and René Pailler, University Bordeaux, 33600 Pessac, France

Hypothetically, if it were somehow possible to fully saturate the residual ~13% porosity with β-SiC (disregarding threshold porosities for the moment), the densified composite would contain zero open porosity, the bulk density and true density would coincide and the final composite bulk density would become . . . $\rho_{b,14}$ = 2.17 g/cc. But this is not possible because threshold porosities limit complete densification. At any rate, since the tool is out and being used, consider some scenarios in which the HS40 preform (substrate) is densified exclusively with a single matrix material throughout, that is, from the preform state $i = -2$ to the final $i = 13$ state. Ignoring rigidization requirements for the moment, recall that the bulk density and open porosity for the undensified, freshly woven preform are $\rho_{b,-2}$ = 0.81 g/cc and $p_{o,-2} = 1 - f_v = 56.4\%$ as provided earlier. These parameters become the starting point for generating the estimates or scenarios given in Table 8 below . . .

Table 8. Final bulk composite densities expected for HS40 substrates densified with a single matrix material.

Densification from the state i = -2 to the state i = 13

Matrix	**Cured Phenolic**	**Glassy Carbon**	**Pitch Carbon**	**Pitch Carbon**	**Pyro Carbon**	**β-SiC**
Method	molded	PIP	PIP	PIP/graph	CVI	CVI
Threshold p_t	p_t ~ 4%	p_t ~ 8%	p_t ~ 10%	p_t ~ 12%	p_t ~ 12%	p_t ~ 12%
Final ρ_b	1.46 g/cc	1.51 g/cc	1.43 g/cc	1.72 g/cc	1.72 g/cc	2.23 g/cc

A couple of additional scenarios have been improvised for Table 8 to represent possible cases in which the preform was simply molded in phenolic resin and another where the carbonized pitch composite was subjected to full graphitization temperatures (4000°- 4500°F) in multiple steps across the process. All in all, these estimates are quite reflective of composite bulk densities reported throughout the literature and are supported by independent studies and resources for similar composite platforms (i.e. . . 3-D carbonized PAN reinforcements embedded in organic/inorganic carbon and SiC matrix systems). The results depicted in Table 8 could provide some interesting insights into the nature of the material if the original HS40 3-D preform was processed along entirely different routes from scratch. This approach could also be expanded to include a mixture of bi-, tri- and quadmatrix scenarios. For instance, using the premise suggested by Eq(2D) above (as taken from Appendix D), a formula for estimating the bulk composite density of the current quadmatrix C-C/SiC system under study might take the form . . .

$$\rho_b = \rho_{b,-2} + (p_{-2} - p_{-1})\rho_{cp} + (p_{-1} - p_0)\rho_{cm} + (p_0 - p_{10})\rho_{s,a} + (p_{10} - p_{13})\rho_{s,\beta}$$

where ρ_{cp} is the density of the carbonized rigidization polymer, ρ_{cm} is that of the carbonized mesophase pitch, $\rho_{s,a}$ the density of a-SiC and $\rho_{s,\beta}$ the density of β-SiC. This approach may provide a quickie means for roughly estimating certain properties in composites comprised of multi-constituent matrices, but it is not nearly as accurate as the method of partial fractions outlined in Appendix B.

Gas-Permeable Porosity: Functional Characterization & Speculations

The open (liquid-permeable) porosity can be physically measured, and so can the gas-permeable porosity (the helium porosity). However, it is difficult to ascertain the fraction of *closed* porosity and hence the *total* porosity in a given material system. As with the open porosity fraction, the partial fraction of porosity that is closed off, sealed up, plugged, blocked, occluded, covered over, impervious or otherwise impermeable to Darcy flow can consist of macro-, meso- and micro-pores, spherical voids, tubular voids, bubbles, inclusions, tunnels, dendrites, cavities, separations, delaminations and microcracks. Glass materials including glassy carbons and glassy ceramics (such as charred phenolic and SMP-10 resins) are known to contain spheroid-shaped bubble-type voids which are completely hermetic to Darcy flow. These types of closed micro-volumes have been confirmed and dimensionally measured using small angle x-ray and neutron diffraction techniques on monolithic samples of these materials.[1]

For certain multi-constituent composite systems, much of the porosity is interconnected, at least through the smallest of micro-channels. Undoubtedly, if all the porosity volume available to infiltrating He atoms was physically quantified, a substantial portion of the total porosity would be captured. Recall Table 1 which outlines various definitions or levels of density for each primary constituent in the C-C/SiC system. The first row in Table 1 contains bulk density values most relevant to flowing liquids (liquid permeable densities) while the second row includes density values susceptible to permeating gases as based on helium volume measurements (x-ray and theoretical densities are more appropriate to electron flow and lattice-scale interactions). Note however, that test results acquired using helium pycnometry techniques provide density and porosity values which include all the liquid-permeable macro and meso-pores *in addition to* all the gas-permeable micro-pores. From a practical perspective, porosity values derived via He pycnometry could be envisioned as the *absolute open porosity*. In some situations, these results can be effectively treated as total porosities, or very near it . . . but this excludes most composite materials, particularly those containing matrices which undergo out-gassing and volumetric changes during curing or conversion processes.

Now consider a scenario in which the porosity volume of interest pertains to that fraction of the total porosity that is permeable to He atoms. This approach can follow the same analysis that was developed previously for the open porosity but using the helium densities instead. From Table 1, the following He densities for the each of the C-C/SiC constituents can be utilized: (1) ρ_f ~ 1.95 g/cc, (2) ρ_{cp} ~ 1.8 g/cc, (3) ρ_{cm} ~ 2.0 g/cc, (4) ρ_a ~ 2.8 g/cc, and (5) ρ_β ~ 3.1 g/cc respectively for the HS40 carbon fiber, carbonized rigidization polymer, carbonized mesophase resin, amorphous a-SiC and crystallized β-SiC. Justifications for these assignments are as follows . . .

(1) Many of the bundle intersections, inter- and intra-bundle voids, cavities and interstitials which eventually become impermeable to intruding liquids are actually accessible through micro-channels, allowing passage of He atoms. As a consequence, this is expected to raise the effective fiber (bundle) density substantially. (2) When fully cured/crosslinked thermoset polymers are fired, the ejected pyrolysis gases (primarily hydrogen along with H_20, CO_2, CO, a number of small aliphatics and aromatics) augment the interconnecting network of micro-pores and passages throughout the glassy body but a substantial fraction of closed voids are also created during conversion from organic to inorganic

[1] "Small-Angle X-Ray Scattering from Glassy Carbon", W. S. Rothwell, J. Appl. Phys. 39, 1840 (1968)
[1] "The Effects of Particle Size on Small Angle Neutron Scattering From a Granular Phenolic Resin Char", J.M. Calo & P.J. Hall, Strathclyde University, Scotland, UK

carbon. As referenced earlier, the evidence clearly shows that many of these enclosed volumes are hermetic to gases and liquids. Thus, the He density is not expected to be much different than its liquid-permeable density. (3) As with glassy carbons, when pitch mesophase resin carbonizes, the interconnecting porosity network is broadened. Unlike glassy carbons however, this conversion process is *not* accompanied by the formation of hermetically sealed bubbles. In combination with volumetric shrinkage due to microstructural condensation and compaction, these two effects cause the apparent density to approach theoretical. (4) Amorphous (glassy) a-SiC formed via low-temperature pyrolysis is expected to exhibit an appreciable degree of gas hermeticity analogous to the glassy carbons with only a slight increase in density because many of the closed voids are inaccessible to He atoms. (5) β-SiC formed from high temperature pyrolysis of a-SiC will have most of the formerly closed pores and voids opened up and rendered accessible to the outside as it undergoes close to 50% volumetric shrinkage, so its density will tend to approach that of true SiC.

Now, while the bulk density of the dry preform remains the same as before, the corresponding fiber volume fraction does not. At the state $i = -2$, the new fiber volume becomes . . .

$$f_v = f_{w,-2}\frac{\rho_{b,-2}}{\rho_f} = \frac{0.81\ \text{g/cc}}{1.95\ \text{g/cc}} \approx 41.4\%$$

Consulting Eq(8A) from the previous section . . . $p_{o,i} = 1-\rho_{b,i}\rho_{m,i}^{-1} - f_v\left(1-\rho_f\rho_{m,i}^{-1}\right)$ along with the results generated in Appendices B and C, it becomes obvious that substantial changes in the complex matrix density will occur when all the helium densities are factored in. Using these new parameters, a plot of the He porosity as well as the most appropriate model function can be developed, similar to the open porosity given earlier. These results are depicted in Figure 5 below, followed by Table 9 which contains values for selected states of interest.

Figure 5. Helium porosity and model fit across the process based on He density expectations.

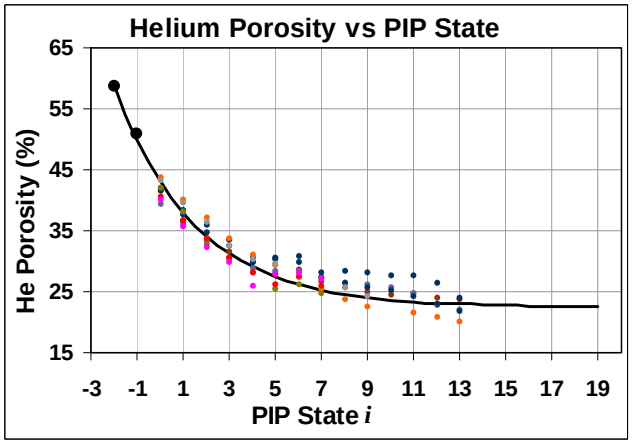

$$p_{He,i} = 20.6\,e^{-0.283i} + 22.4$$

Table 9. Selected points of interest along the C-C/SiC total porosity model curve.

Helium Porosity

Dry Preform State i = -2	Rigidization State i = -1	Carbon Pitch State i = 0	1st Ceramic State i = 1	5th Ceramic State i = 5	10th Ceramic State i = 10	13th Ceramic State i = 13	∞th Ceramic State i = ∞
58.8 %	49.8 %	43.0 %	38.0 %	27.4 %	23.7 %	23.0 %	22.4 %

At the carbon state $i = 0$, the average helium porosity fraction is indicated to be on the order $p_{He,0}$ = 20.6 + 22.4 = 43.0%, while its value after infinite densification bottoms out at a 'helium' threshold porosity of $p_{He,\infty}$ = 22.4%. Also note that at $i = 13$, $p_{He,13}$ = 23.0% which is substantially higher than the $p_{o,13}$ = 13.0% value already established as the average residual open porosity for fully densified C-C/SiC substrate. The difference between these two, 10%, cannot be correctly associated with the partial fraction of the total porosity that is hermetically sealed. However, it is certainly representative of the micro-porous interconnecting network that was impermeable to liquids, but more importantly . . . it includes all the voids and pores within that network which were formerly recognized as closed and inaccessible. Analogous to the true (liquid-impermeable) density defined earlier, the true He-impermeable density pertains to the fraction of material that is impermeable or impervious to gases as defined by [1] . . . $\rho_b = (1 - p_o)\rho_t$.

Theoretical or Absolute Porosity: Properties & Speculations

The concept of theoretical (absolute) porosity bears little relevance to practical material properties but is explored here as an introspective exercise to compare with the other porosity levels and perhaps to facilitate a better understanding of the term 'total porosity'. Obviously, this would include all liquid and gas-permeable porosity subject to Darcy flow along with all the hermetically sealed voids and micro-channels which were previously impossible to breach but may be susceptible to Fickian diffusion. The absolute porosity would also include tubular pores and shielded voids in- between fiber filaments (intra-bundle porosity), porosities and certain surface morphological features within the individual fiber filaments (fiber porosity), microstructural defects, imperfections and dislocations, crystalline/lattice holes and interstitials, etc . . . In accordance with the methods applied above for the open and helium porosities, the theoretical porosity data plot and most appropriate model fir are given below followed by tabulation of selected values of interest . . .

Figure 6. Absolute porosity and model fit across the process based on theoretical constituent densities.

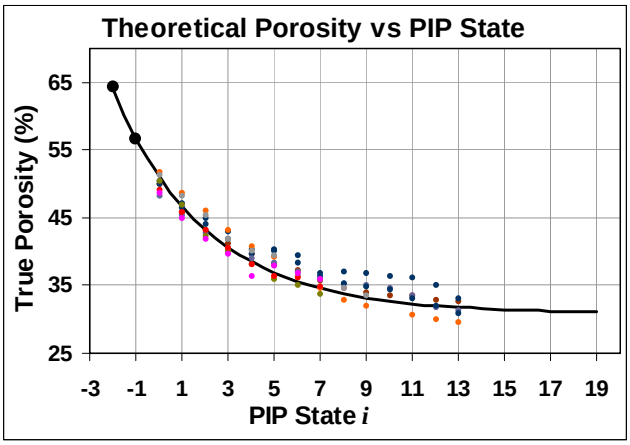

$$p_{Abs,i} = 20.2\, e^{-0.245i} + 30.9$$

Table 10. Selected points of interest along the C-C/SiC absolute porosity model curve.

Theoretical or Absolute Porosity

Dry Preform State i = -2	Rigidization State i = -1	Carbon Pitch State i = 0	1st Ceramic State i = 1	5th Ceramic State i = 5	10th Ceramic State i = 10	13th Ceramic State i = 13	∞th Ceramic State i = ∞
63.8 %	53.7 %	51.1 %	46.7 %	36.9 %	32.7 %	31.8 %	30.9 %

The potential implications from these results include a 'true' fiber volume fraction in the mid thirties (compare with the original bulk fiber volume of ~44%), a total matrix volume at i = 13 of about 33% (compare with the original matrix volume of about 43%), and a potential closed (liquid-impermeable) porosity fraction at the end of the process of ~20%! For graphical comparison, Figure 7 gives a side-by-side plot of all three porosity functions illustrating their behavior across the process.

Figure 7. Model plots of the liquid, gas and absolute porosities for C-C/SiC across the densification process

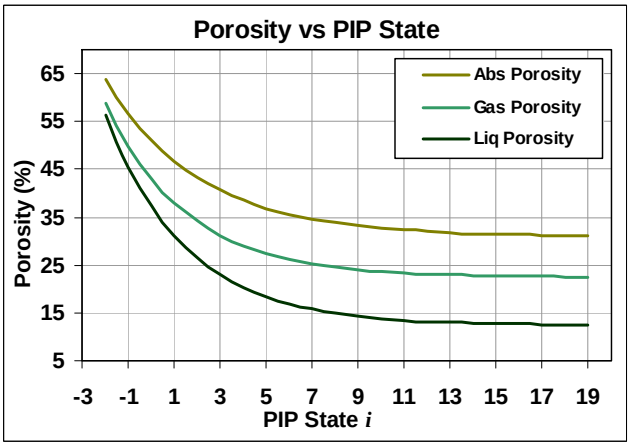

True Densities: Survey & Comparisons

Each porosity level has its own 'true' density associated with it. The 'bulk' density is simply the weight divided by the geometrical volume. It includes the total porosity of the system. The first true density excludes the liquid-permeable porosity and is impermeable to liquids, the second true density excludes the gas-permeable porosity and is impermeable to gases while the theoretical density (the absolute or perfect crystal density) is the ultimate true density of a material, in theory. This latter true density is not so practical in everyday industrial materials engineering. For comparison purposes, the four density levels of interest are plotted side-by-side in Figure 8 . . .

Figure 8. Model plots of the four levels of density relevant to the C-C/SiC system across the densification process

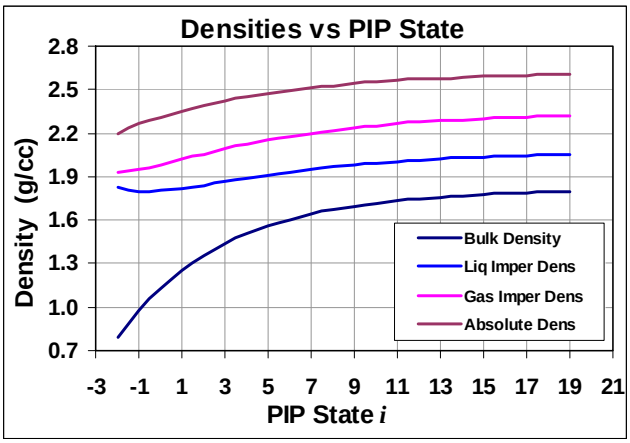

It is obvious for the C-C/SiC system, that the bulk density will never even come close to its true density (the liquid-impervious density) since both increase similarly and approach asymptotes well distanced from each other. This is in line with previous results showing that the threshold open porosity is not a small number (> 10%) – the open porosity will always represent a significant volume fraction entrenched within the material, even after many, many densification cycles are applied. Any speculations that the C-C/SiC material could be processed up into the 2.5-2.8 g/cc range or above are ambiguous. This is in accordance with the results derived earlier for Tables 7 and 8. It is obvious that threshold levels for both liquid and gas-permeable densities (which are unattainable in the first place) track substantially above the bulk density and are well out of the reach of physical processability.

Section IV (Preceramic SiC Densification)

Selected excerpts taken from **"Density, Porosity & Constituent Fractions in C-C/SiC"**, *Randy Lee*

Estimation of Complex Composite Matrix Densities for the C-C/SiC System

It is extremely difficult to physically measure the density of multi-fractional matrices within most composite systems, particularly carbon and ceramic matrix systems. More importantly, it is physically impossible to directly ascertain the matrix density in the C-C/SiC system which changes from state-to-state. Thus, astute estimation methods must be employed, and even these approaches are difficult to accurately execute with any appreciable degree of confidence that the results will be meaningful and realistic. However, with the information that is now at hand, this task becomes quite feasible. The potential value associated with this type of analysis can provide a unique and critical piece of the puzzle needed to effectively characterize and quantify specialized material properties which can often only be speculated on.

During the early process stages, the C-C/SiC matrix consists only of inorganic carbon. By the end of the densification process, the matrix contains four co-constituents or partial fractions in which each has its own unique bulk and true density. However, in accordance with the principles set forth by the fundamental composite relationships implied in Eq(1A) and (5A), these complex matrix densities can be reasonably estimated if the fractional weight coefficients for each constituent are known to a reasonably accurate degree. Relevant fractional quantities were determined in Appendix B. Now, if the open porosity fraction in Eq(5A) is taken to zero, the resulting net density becomes a representative function of the particular densities utilized for the co-constituents. For instance, the use of co-constituent bulk densities (that is, liquid-permeable densities), provides an expression for estimating the net bulk (liquid-permeable) density of the complex matrix, that is . . .

(1C) $$\rho_{m,i} = \left(c_{p,i}\, \rho_{cp}^{-1} + c_{m,i}\, \rho_{cm}^{-1} + s_{a,i}\, \rho_{a\text{-}SiC}^{-1} + s_{\beta,i}\, \rho_{\beta\text{-}SiC}^{-1} \right)^{-1}$$

where $c_{p,i}$, $c_{m,i}$, $s_{a,i}$ and $s_{\beta,i}$ are the fractional weight coefficients for carbonized rigidization polymer, carbonized pitch mesophase, amorphous (glassy) SiC and crystalline SiC respectively at any state of interest i, along with their corresponding bulk densities (as provided in Table 1 near the beginning of the report), namely, ρ_{cp} = 1.45 g/cc, ρ_{cm} = 1.35 g/cc, $\rho_{a\text{-}SiC}$ = 2.45 g/cc and $\rho_{\beta\text{-}SiC}$ = 2.95 g/c , which are considered to be the effective densities relevant to all liquid impregnations, intrusions and infiltrations.

Table 1C below provides estimates for the net matrix bulk density across the densification process based on the previously determined partial matrix fractions and the corresponding co-constituent matrix bulk density averages from Table 1. This is followed by a graphical plot of these results in Figure 1C.

Table 1C. Net matrix bulk density estimated from partial matrix weight fractions and co-constituent matrix bulk densities.

Process State *i*	-1	0	1	2	3	4	5	3000°HT	6	7	8	9	10	3000°HT	11	12	13
Matrix Bulk Density (g/cc)	1.45	1.40	1.57	1.69	1.78	1.87	1.89	2.06	2.08	2.10	2.10	2.11	2.11	2.15	2.16	2.17	2.18

Figure 1C. Graphical depiction of the bulk matrix density for the C-C/SiC system as it changes across the densification process.

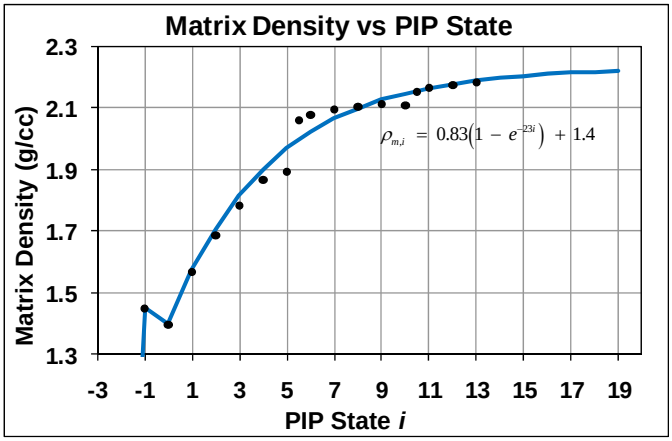

While this data does not exactly lend itself to accurate or meaningful curve modeling, there is an indication that the maximum bulk matrix density tends to approach ~ 2.23 g.cc after infinite densification. Now, this is the matrix density under the scenario or pretense that the open composite porosity fraction is completely contained within the matrix volume. Obviously, this is slightly over-simplistic but the approach has demonstrated valid results for a number of composite systems. From another perspective, net bulk matrix densities would be even lower if some of the *closed* porosity fraction was also sealed within the matrix. For example, the true (liquid-impervious) matrix volume at the state i = 13 is around ~43% but with inclusion of the ~13% average open composite porosity, the bulk matrix volume comes closer to ~56%. However, this is a misnomer since the ~13% porosity is open. If absolute densities for each of the matrix constituents were considered (that is, 2.26 for carbon and 3.21 for SiC) resulting in a total porosity of about ~23%, the net matrix bulk density would be substantially lower. In any case, the liquid impervious matrix volume is still ~43% and the true matrix density remains unchanged regardless. Open and closed porosity may sometimes seem like a world apart in terms of accessibility and permeability but geographically, these pores may only be separated by a few angstroms across a thin wall of matrix material which just happens to be stout, impervious and isolated from the immediate local surroundings.

Selected excerpts taken from **"Density, Porosity & Constituent Fractions in C-C/SiC"**, *Randy Lee*

Estimation of Densities for Hypothetical Cases in the C-C/SiC System

It is interesting to speculate on what the final substrate density might be if the material were completely densified with carbonized pitch matrix throughout, or if it were densified exclusively with β-SiC, or . . . if the ~13.4% remnant porosity characteristic of the fully densified substrate at i = 13 were somehow completely filled with one of these matrix materials. Speculation densities for this system are not difficult to estimate given all the other information that is now available. First however, briefly examine how each constituent changes as the substrate is processed through the succession of densification cycles by re-evaluating the development of Eq(1A) and Eq(4A) given in Section II. Using the symbols . . . ↑ to designate an 'increasing' variable; ↓ for 'decreasing'; and — for 'no change', it can be visualized how the bulk density of the substrate increases only because specific constituents increase while other constituents either decrease less or do not change at all. Consider the concerted forms of Eq(1A) and Eq(4A) . . .

$$\underset{\uparrow}{\rho_b} = \underset{\uparrow}{\frac{W}{V}} = \underset{\uparrow}{\frac{w_f + w_m}{v_f + v_m + v_p}} = \underset{\downarrow}{f_v}\underset{\uparrow}{\rho_f} + \underset{\uparrow}{m_v}\underset{\uparrow}{\rho_m} = \underset{\downarrow}{\left(f_w \rho_f^{-1} + m_w \rho_m^{-1}\right)^{-1}}\underset{\downarrow}{(1-p)}$$

$$\underset{—}{} \quad \underset{—}{\phantom{\frac{W}{V}}} \quad \underset{\uparrow}{\phantom{\frac{w_f + w_m}{v_f + v_m + v_p}}} \quad \underset{\downarrow}{}$$

Volume Fractions *Weight Fractions*

Not surprisingly, the raw matrix volume increases at the expense of the porosity volume while the total (raw) volume of the article or panel remains constant. This is also reflected in the fractional expressions.

Now, consider the increase in bulk density due to an incremental weight quantity w_x introduced into the remnant pores of the substrate above and beyond the matrix weight which is already present w_m, that is . . .

$$\underset{—\ —\ \uparrow}{\rho_b} = \underset{—\ —\ \uparrow}{\frac{w_f + w_m + w_x}{V}} = \underset{—\ —\ \uparrow}{\frac{w_f + w_m}{V}} + \underset{\uparrow\ —}{\frac{v_x \rho_x}{V}} = \underset{—\ —\ —\ \uparrow}{\frac{w_f + w_m}{V}} + \rho_x x_v$$

. . . and so the change in the bulk density is due only to weight contributed by the partial volume fraction of the new material x_v as it occupies the existing pore volume, as given simply by . . .

$$d\rho_b = \rho_x d x_v$$

In general, the bulk density at any future state ρ_b can be estimated simply by appending the bulk density at a previous state $\rho_{b,o}$ with the density contribution from the new material $x_v \rho_x$, that is . . .

(1D) $$\rho_b = \rho_{b,o} + x_v \rho_x$$

where ρ_x is the density of the new material and x_v is the volume fraction of the same. For the purposes intended here, x_v might represent the former open porosity now occupied by the new material, or at least, a portion of the open porosity . . . since the porosity asymptotically approaches a minimum limit or threshold, even after many densification cycles, it is physically impossible to attain zero porosity with these types of material systems. Consider the following examples. It has now been inferred that the threshold porosity for the FMI C-C/SiC system approaches ~12%, while threshold porosities for 2-D laminated and 3-D braided phenolic-densified C/C forms have been independently confirmed to approach ~3% and ~8% respectively.

Threshold porosity p_t can also be considered as unavailable porosity due to the constrictions of the material system being densified. Thus, it can be accounted for in Eq(1D) simply by modifying the pore volume available to the densifying material, that is . . .

(2D) $$\rho_b = \rho_{b,o} + \left(x_v - p_t\right)\rho_x$$

For the sake of curiosity, consider first situations in which the remaining 13% porosity in the C-C/SiC substrate were carried to full theoretical density, being densified say with β-SiC, or carbonized pitch or pyrolytic carbon. This act would constitute a 14th densification cycle carrying the substrate to the i = 14 state. While it is physically impossible to attain zero porosity with PIP-type (liquid-densified) substrates, including essentially all C/C and CMC forms, it is interesting to wonder what the final density might be if all the residual porosity at the state i = 13 were fully saturated with β-SiC or carbonized pitch.

Evidence for the C-C/SiC system under study indicates that the average threshold open porosity is very close to 13% for liquid densification using SMP-10 carbosilane resin low fired to the a-SiC state. Phenolic/furfurylol liquid-densified systems such RCC and ACC have been proven to exhibit a threshold porosity of about ~3%, which is probably comparable to pitch-densified approaches as well. However, it has been shown that the fraction of closed porosity increases with excessive liquid-densification cycles, and the formation of closed porosity has also been demonstrated during CVD/CVI densifications when the process parameters are not fully optimized. Using Eq(2D), various scenarios can be estimated as given in the table below and further elaborated on in Tables 7 and 8 on pages 18 and 19 in the report.

Glassy Carbon[1] ρ_b = 1.45	Pitch Carbon[2] ρ_b = 1.35	a-SiC ρ_b = 2.45	β-SiC ρ_b = 2.95	β-SiC ρ_b = 3.21	Kerosene $\rho_b = 0.817^{77°F}$	Water $\rho_b = 0.998^{77°F}$	Phenolic Resin[3] ρ_b = 1.24
1.94 g/cc	1.92 g/cc	2.07 g/cc	2.14 g/cc	2.17 g/cc	1.85 g/cc	1.88 g/cc	1.91 g/cc

Section VI (Preceramic PolyCarbosilanes: Reactions & Mechanisms)

Selected excerpts taken from **"PolyCarbosilanes: Reactions & Mechanisms"**, *Randy Lee*

In general, freshly synthesized versions of most of these polymers (or oligomers), as well as their semi-organic, *carbide*-modified versions (ex. Ceraset silazane and Blackglas siloxane) tend to form ring-like structures during the synthesis process. A couple of examples might include the following structural representations (branched carbosilanes are slightly different and will be covered in the next section) . . .

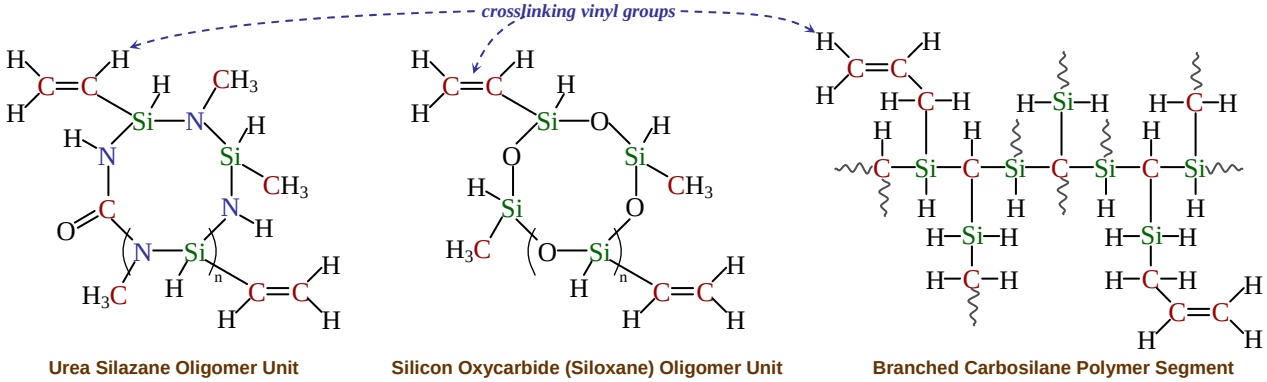

Urea Silazane Oligomer Unit **Silicon Oxycarbide (Siloxane) Oligomer Unit** **Branched Carbosilane Polymer Segment**

Pyrolysis of silazanes in 100% argon atmosphere yields silicon-based ceramic products which are a mixture of the carbide and the nitride . . . SiC/Si_3N_4. However, when the gas mixture includes increasing levels of reactive ('spoiler') gases, such as hydrogen or nitrogen, the product can be tailored to favor SiC or Si_3N_4. High fire pyrolysis (> ~2500°F) in 100% H_2 gas yields 100% β-SiC, while the same pyrolysis cycle carried out in 100% N_2 or heavy NH_3 would yield 100% Si_3N_4. These results and effects have been personally verified experimentally during extensive studies with these materials.

Preceramic siloxanes, $HO[–SiR_2O–]_nH$, are typically prepared through a sol-gel process. Pyrolysis of these cured materials in 100% Ar gas yields a classic silicon oxycarbide product (SiO_xC_y) which many analytical tools often perceive as $SiC\text{-}SiO_2$ structural mixtures. Incorporation of 'free' carbon into the microstructure 'blackens' the product (ie... Blackglas). Pyrolysis in heavy H_2 atmospheres will ultimately produce SiC, however, this negates the intention of using siloxanes in the first place (more viable precursors are readily available for direct formation of SiC). Similarly, when inertly produced silicon oxycarbide products are subsequently subjected to high temperature treatments or excursions (> ~2400°-2500°F), the $SiC\text{-}SiO_2$ glass structure begins to reduce down to β-SiC with substantial reductions in volume (this is indicative of the temperature limitation for these materials). Post-fire treatment temperatures can be substantially lowered when H_2 gas is utilized as a reducing/dehydration agent (oxygen scavenger) in the post-fire atmosphere. This is illustrated below for the conversion of cured silioxane resin into silicon oxycarbide (glassy) ceramic and then to a-SiC glassy ceramic . . .

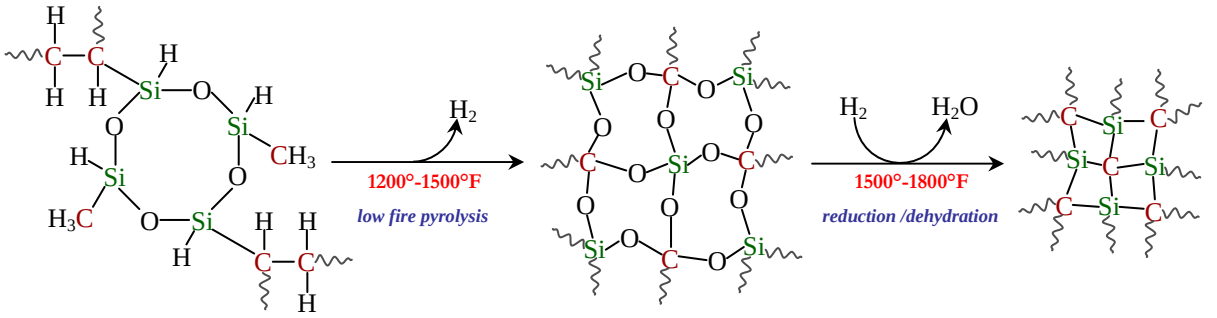

Crosslinked Siloxane Resin **Glassy Silicon Oxycarbide Ceramic** **Glassy a-SiC Ceramic**

Treatment to > 2000°-2200° would crystallize the a-SiC into β-SiC with further (drastic) reductions in overall volume (30-40% as indicated above) along with the accompanying porosity development. Thus, in reducing atmospheres (such as certain solid fuel nozzle environments), the oxycarbides may be expected to experience significant volume shrinkage and porosity creation, but in oxidizing environments (such as the skins and leading edges of lower orbit vehicles), these materials will tend to exhibit a certain degree of relative inertness with much more stability. Oxycarbides would likely demonstrate undesirable effects in reducing NH_3 ammonia environments as well. Effective incorporation of boron into the SiO_xC_y structure has been demonstrated to increase the oxidation protection of these materials.

SYNTHESIS OF SMP-10 ALLYL HYDRIDO POLYCARBOSILANE RESIN

Carbosilanes comprise the family of semi-organic polymer resins characterized by a molecular configuration in which carbon and silicon atoms are covalently bonded directly to one another in an alternating fashion along the primary polymer chain segments . . .

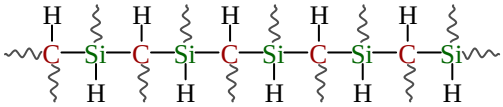

Note: ∿∿ simply means a continuation of the structure not shown

alternating sequence of carbon-silicon atoms along a linear segment or chain in a carbosilane polymer/oligomer

Additionally, these methylene-linked silicon structures are typically comprised of linear segments which are highly branched, with little cyclization. Obviously, the regional 'closeness' of carbon and silicon atoms along the virgin chain facilitates the formation of near-stoichiometric SiC in the final pyrolyzed product (indeed, the two atoms are already bonded together in semi-organic form). However, formation of any kind of polymer which can readily transform into stoichiometric SiC upon firing is no small accomplishment. The particular synthesis approach developed by Starfire Systems to make SMP-10 is unknown or ambiguous at best. Long time personal associations with the principal founder and developer of Starfire SMP-10 polymer has permitted opportunities to keep abreast of certain technological aspects and to track the history of this unique material as it has undergone improvements and refinements over the years. It is known that Starfire scientists worked several years to develop a synthesis method that was consistent and fruitful, and they had to overcome many problems before finally refining the techniques that led to their first marketed product, allyl hydrido polycarbosilane, or AHPCS for short.

The particular carbosilanes of interest here involve two stages of resin synthesis . . . formation of the hyperbranched carbosilane oligomer backbone and then the attachment of unsaturated pendant side groups. These unsaturated side groups allow the end user to cure (harden) the material prior to pyrolytic ceramicization by inducing crosslinking reactions between neighboring polymer branches. This two stage approach is not uncommon in the various fields of organic thermosets (ex. acrylic or styrene monomer crosslinked polyester resins are widely used as commercial fiberglass resins and coating lacquers). It is also known that Starfire workers experienced great challenges during development activities associated with the second stage of the synthesis process. Much effort was expended in attempts to attach common vinyl groups to open branches within the carbosilane polymer network which would facilitate subsequent

crosslinking in an effective and consistent manner. Eventually, proper incorporation of *allyl* groups led to the successful product sold as AHPCS polymer (note that allyl = propenyl = methyl vinyl).

Minor refinements in the polymer structure along with more fashionable trade name nomenclature for their growing line of AHPCS-based products eventually led to the now famous SMP-10 polymer which is, at the very least, the basic ingredient for the company's primary line of product offerings (in order to avoid confusion, it should be realized that SMP-10 *is* AHPCS). Products offered by Starfire based on SMP-10 polymer range from ultra-low viscosity CVD polymers to liquid fiber coating dips to composite matrix resins and slurries. Understandably, the specific techniques and reaction pathways employed to synthesize AHPCS/SMP-10 polymer have generally been proprietary. However, techniques for attaching carbon atoms directly to silicon can be surmised given the vast resource of potential reaction scenarios defined in the field of organic chemistry. Of particular interest here are the reaction approaches involving Grignard reagents and *Grignard synthesis*. Grignard agents are haloorganometallic compounds (or molecular segments) which induce coupling with another molecule, end-segment or agent containing halogen. For most applications, the Grignard functional group consists of magnesium chloride, R_1–MgCl, while chloride is also the halogen attached to the co-reactant R_2–Cl. These –MgCl agents are very reactive, as they will react readily with H_2O, CO_2, O_2, NH_3 and many other organic/inorganic functional groups. Grignard reactions must be conducted under completely anhydrous conditions.

Grignard agents are unique to organic carbon since the carbon atom attracts electrons from the electropositive magnesium atom forming a covalent bond between the two, while the magnesium and chloride atoms ionically bond together. This organometallic complex exhibits high polarity. Other metals (such as copper and lithium) as well as the other halogens (Br and I) can also form Grignard reagents, depending on the desired effects. Of special interest here is the reaction between the family of magnesium chloromethanes and those of the chlorosilanes as a starting point for carbosilane synthesis as depicted below. Here, a silyl chloride attacks the MgCl group causing silicon to become slightly positive while carbon becomes negative (a carbanion). As the two entities combine, $MgCl_2$ is ejected . . .

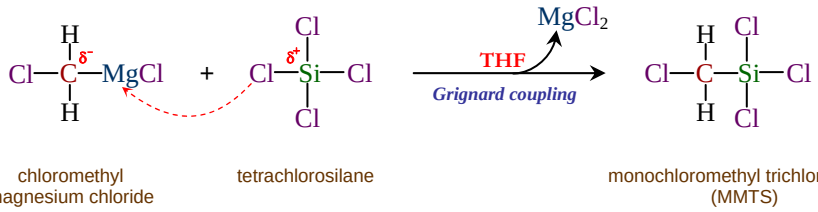

The product of this reaction, monochloromethyl trichlorosilane (MMTS) is considered to be the primary reactive monomer ultimately leading the formation of polycarbosilane. It can be surmised that the di- and tri- chlorinated versions of both the methyl and silyl reactants are also synthesized and strategically incorporated into the reaction mixture at controlled levels to influence the nature, frequency, content and length of branching throughout the growing molecule. For the intended purposes here, MMTS can be used to illustrate the typical reaction pathway leading to the highly branched, chlorinated carbosilane first stage polymer via Grignard synthesis . . .

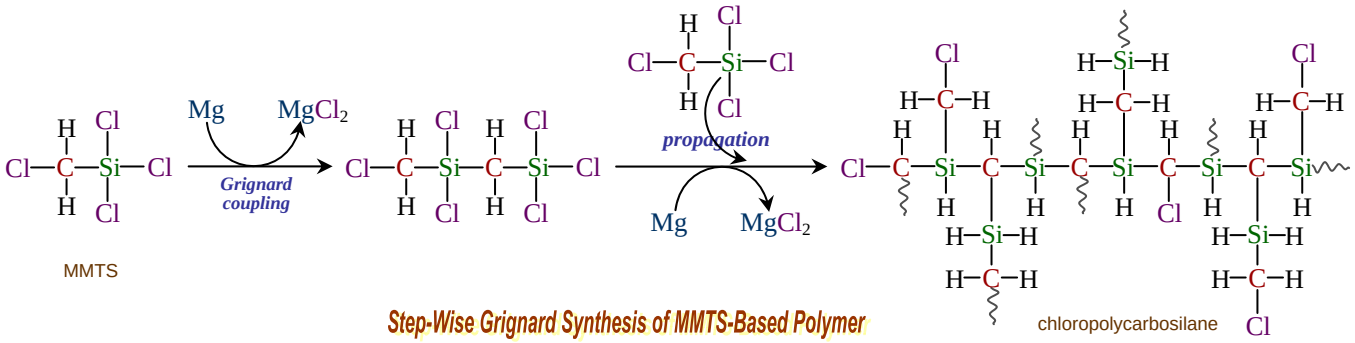

Step-Wise Grignard Synthesis of MMTS-Based Polymer

As can be seen, this intermediate product is laden with residual chlorine in which –Cl groups are retained at most of the unreacted sites. Ultimately, all these chloride groups must be extracted from the system and this can be accomplished by treatment of the chlorinated polymer with the appropriate reducing agent. However, before reduction operations are implemented, it should be recognized that these –Cl groups are key to providing an attractive and compatible method for incorporation of the allyl crosslinking groups into the macromolecule.

Independent resources have indicated that the allyl content in as-received AHPCS/SMP-10 polymer runs around 10 to 15%. During the second stage of the synthesis process (attachment of the allyl groups), it can be surmised that some of the objectives are to . . . (a) incorporate a few of these groups along the outer fringes of the polymer clusters, (b) avoid excessive allylation of the polymer adduct, (c) ensure uniform distributions of allyl groups throughout the branches of each macromolecular cluster, and (d) prevent allyl groups from penetrating deep into the polymer core where their reactive effects may be sterically hindered later on. It should be noted that each incorporated allyl group changes the Si:C stoichiometric balance of the ceramic precursor, and every group that is added in excess of the molecular design strategy will inevitably lead to a 'carbon rich' ceramic product. Undoubtedly, it was essential for Starfire scientists to develop a rather innovative technique to effectively distribute the optimum level of allyl (propenyl) groups at the desired positions along the polymer periphery.

There are at least two possible pathways capable of facilitating the attachment of allyl pendant groups onto the intermediate polymer end-branches. One approach involves a mechanism of free radical substitution directly utilizing propene to incorporate the allyl groups. As propene gas is bubbled through the chlorinated polymer mixture at elevated temperatures, HCl gas is generated when allylic carbon displaces chlorine in the mother structure. A possible scenario for the attachment of allylic (propenyl) groups onto end-braches in the chlorinated polymer via free radical substitution might be . . .

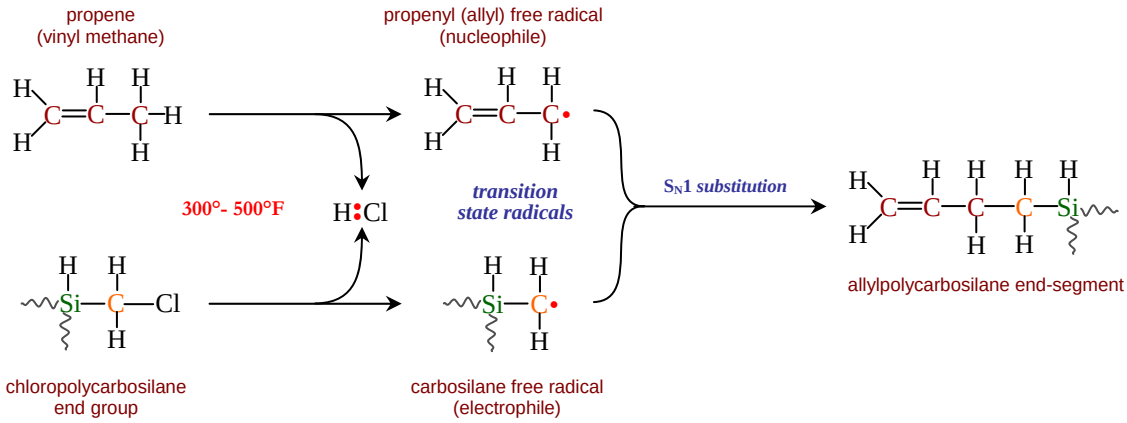

Here, propene and the chlorocarbon end-group dissociate into their respective free radicals where the nucleophillic propenyl radical couples with available (unhindered) electrophillic carbosilane radical end-groups. Chloride functions as the 'leaving group' and the reaction mechanism is expected to favor S_N1 kinetics over S_N2 because . . . (a) steric hindrance is significant due to the structural shielding effect imparted by the highly branched polymer (poor access to reaction sites discourages backside attack and chiral inversion which are characteristic of S_N2 substitution), (b) chloride is a relatively strong base (weak basic leaving groups favor S_N2 substitution), and (c) the reaction is likely carried out in an aprotic solvent such as tetrahydrofuran (THF) or dialkyl ether (protic solvents such as water and alcohols are characterized by hydrogen bonding which tend to favor S_N2 kinetics).

Note 1: An allylic carbon atom is one that is adjacent to a double bond . . . it is the alpha carbon directly attached to the vinylic carbon which forms half of the double bond in a vinyl group. Propene (or vinyl methane) is the simplest allylic compound. Due to resonance, allyl compounds readily form very stable radicals (low bond dissociation energy) which accounts for their high reactivity towards substitution. However, ionic addition to the double bond is a competing reaction which must be minimized by careful control of the reaction conditions. As the nucleophillic propenyl radical is formed, bonding between all three carbon atoms is converted from sp^3 hybridized σ orbitals to sp^2 σ–π combined orbitals (a nucleophile is a negative reactant seeking a cation). In general, the symmetric allyl radical is a hybrid of two equivalent resonance structures where the π bond and the unpaired electron are delocalized across the entire molecule allowing substitution to occur at either end-carbon.

Note 2: The acronym S_N1 refers to substitution-type reaction mechanisms which follow first order (unimolecular) kinetics and which involve one but sometimes both nucleophillic and electrophillic reactants to varying degrees. The primary reactant of interest in most of these cases is the negatively charged nucleophile (which seeks a nucleus) and determines the overall rate of the reaction. So the term S_N1 stands for unimolecular nucleophillic substitution. In contrast, substitution reactions which involve less structurally complex (branched) reactants (where steric factors are less significant) and weaker basic leaving groups often tend to involve both reactants significantly (opposite to nucleophiles, electrophiles are attracted to negative entities rich in electrons). This leads to second order reaction kinetics whose rate is dependent equally on the concentration of both reactants. Such cases are designated by S_N2 which stands for bimolecular nucleophillic substitution.

The other possible scenario for attaching allyl groups to polymer end-branches within the reaction mixture calls for utilizing the *allyl Grignard reagent*. Again, during the transition state, magnesium Mg^{+2} is attacked by chloride Cl^- causing the end carbon on the polymer to become an electrophillic carbocation which reacts with the nucleophillic alpha carbon in the allyl Grignard agent (the alpha carbon becomes a carbanion), and as the two reactants join together, magnesium chloride is expelled as a by-product . . .

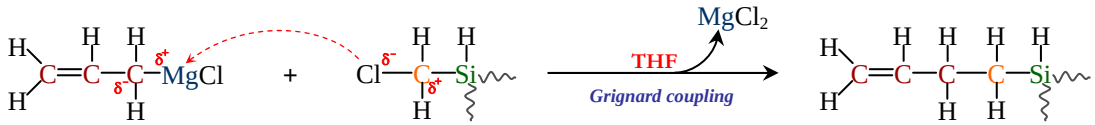

propenyl (allyl) magnesium chloride

chloropolycarbosilane end group

allylpolycarbosilane end-segment

After incorporation of the crosslinking groups has been successfully completed (the goal is probably about 15-20% allylic substitution), there will be a substantial quantity of residual chloride groups remaining throughout the polymer network which must be eliminated or extracted from the system. Since chloride is a moderate reducing agent, a likely approach for its removal (dehalogenation) is substitution with a stronger hydride-type reducing agent. The most prominent and readily available reducing agent for these types of scenarios is lithium aluminum hydride, $LiAlH_4$.

Alternatively, the reducing agent calcium hydride, CaH_2 may also be feasible for this application. $LiAlH_4$ is more soluble in THF as a reaction medium than the commonly used diethyl ether solvent, while

the solubility of CaH_2 in any solvent is quite limited. Both agents are extremely sensitive to atmospheric moisture and must be used under highly controlled reaction and storage conditions. Unfortunately, both can react violently with chlorocarbon compounds under certain conditions, so Starfire workers must have overcame some steep challenges during development of this step. A likely reaction scenario for dehalogenation of the chlorinated polymer via reduction with $LiAlH_4$ is illustrated below . . .

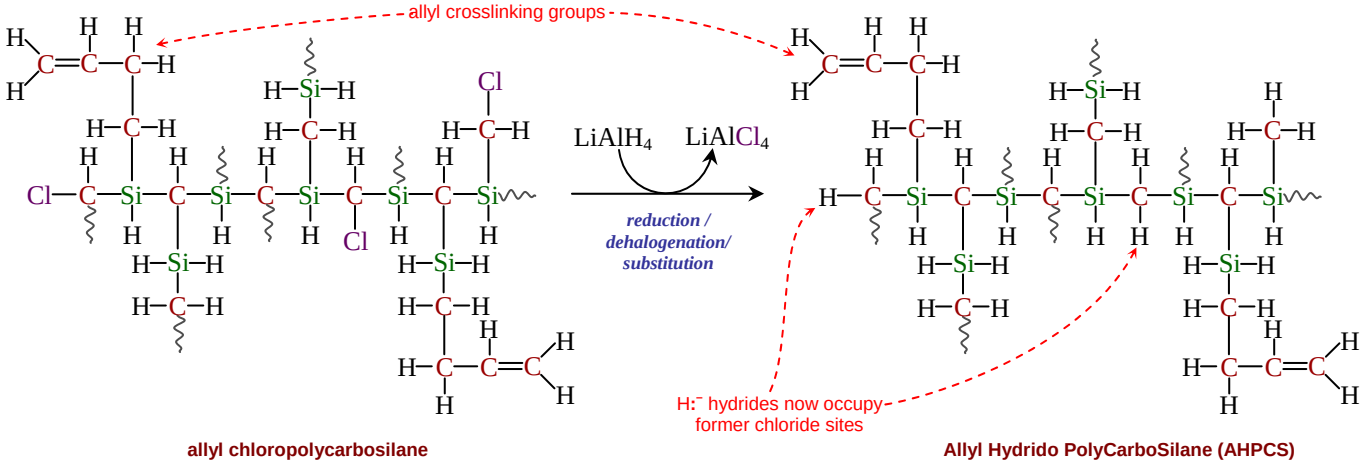

Replacement of the chloride groups with hydrogen atoms, or more specifically, *hydride* $H:^-$ groups, leads to the AHPCS/SMP-10 polymer structure with inclusion of the 'hydrido' nomenclature to the naming system. A hydride group is a negatively charged hydrogen ion, and a very strong reducing agent, which carries two 1*s* electrons, as opposed to a neutral hydrogen atom (radical) containing only one electron, or the more common hydrogen cation H^+ well known for its acidic properties (a solvated proton). Now, reduction/dehalogenation with CaH_2 would proceed according to the same mechanism as that associated with the use of $LiAlH_4$ . . .

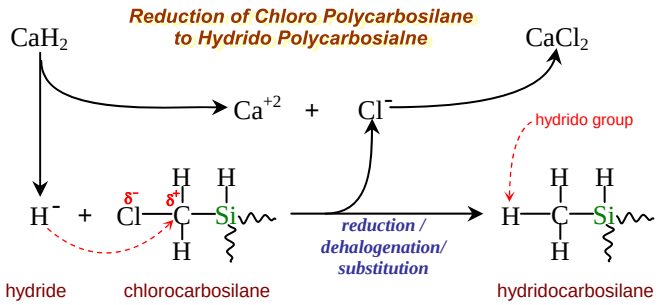

Here, the nucleophillic hydride ion is formed opposite to the more electropositive calcium ion Ca^{+2} (or $LiAl^{+4}$ in the case of $LiAlH_4$) and behaves almost like a halogen or a hydroxyl group displacing chloride from the polymer perhaps following kinetics similar to S_N1. In either case, residual inorganic impurities left behind from the synthesis process, primarily the reduction step (traces of Li, Al and/or Ca), must be cleaned from the system and this is probably done by careful extraction or washing with water. While the respective ions of Li, Al and Ca are readily soluble in water, both of these reducing agents will also undergo hydrolysis, producing effervescing hydrogen gas while the corresponding insoluble hydroxide falls out of solution and is filtered out . . .

$$CaH_2 + 2\,H_2O \xrightarrow{\textit{hydrolysis}} Ca(OH)_2\downarrow + 2\,H_2\uparrow$$

Lastly, a series of drying steps must be applied to the virgin polymer in efforts to remove all traces of water and moisture from the system. A likely drying agent for this purpose is calcium chloride $CaCl_2$. It is well known that these polymers are sensitive to water, which can be absorbed during handling, storage and end-user procedures. Thus, extra caution must be practiced to minimize hydrolytic degradation of the material during the synthesis stages all the way through the final user-application processes.

User Applied Crosslink Processing and Pyrolysis of SMP-10

Before the AHPCS/SMP-10 resin is cured (throughout it's life in the liquid state), the polymer evolves hydrogen gas and remains reaction-sensitive to atmospheric moisture until it is hardened by cure. The cured product continues to emit hydrogen all the way through pyrolysis until it is finally converted into ceramic form. These properties also apply to the silazanes and ureasilazanes covered earlier. In addition, the pre-ceramic resins are very sensitive to acids, bases and catalytic metals, sometimes rapidly expelling H_2 and forming flammable and explosive mixtures in air. Without a doubt, the end-user should develop safe practices and remain cautious during the storage, handling and application of these kinds of resins because hydrogen gassing can result in pressure build-up, fire, and/or explosions.

Hydrogen atoms attached to silicon are not the same as carbon-bound hydrogens. The silicon-to-hydrogen bond is longer and weaker than the carbon-to-hydrogen sigma bond. Silicon-bound hydrogen atoms are so available that many silane compounds, particularly silane itself SiH_4, are often used as reducing agents (ordinary silane, often called silyl hydride, is a strong hydride $H{:}^-$ donator). All compounds containing Si–H bonds can generate hydrogen spontaneously. Additionally, they are hygroscopic, readily absorbing and reacting with environmental moisture and oxygen. Thus, the three less-than-desirable reaction effects associated with these types of liquid pre-ceramic polymers *before* they are ever even subjected to user-applied curing and processing involve . . .

(1) The evolution of hydrogen gas, which is believed to be (partially) due to reactions between neighboring hydrogen-silane segments within the entangled polymer network. Essentially, this is a form of 'crosslinking' between local silyl radicals, and involves the bridging of two silicon atoms . . .

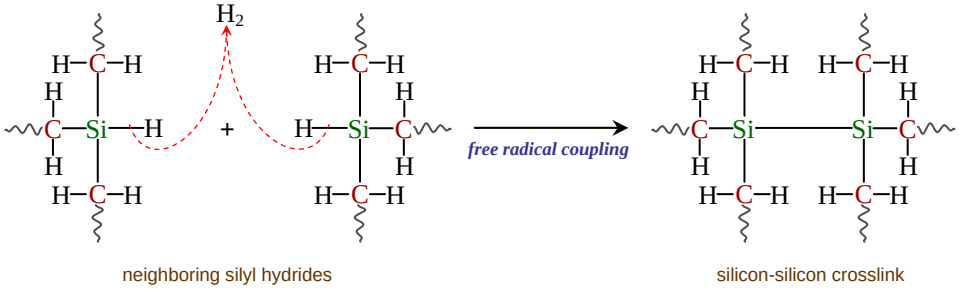

(2) Hydration/hydrolysis of silyl hydride groups along the polymer chain with the formation of silanol groups. Latent residual water within the polymer system and absorption of environmental moisture are the culprits to this effect. The reaction creates hydrogen gas (yet another source of hydrogen generation)

and may proceed along two paths with very different results . . . one facilitating the formation of siloxane linkages between neighboring silanol groups via condensation and the other leading to destructive scission and fragmentation of the polymer chain into alcoholic end-segments . . .

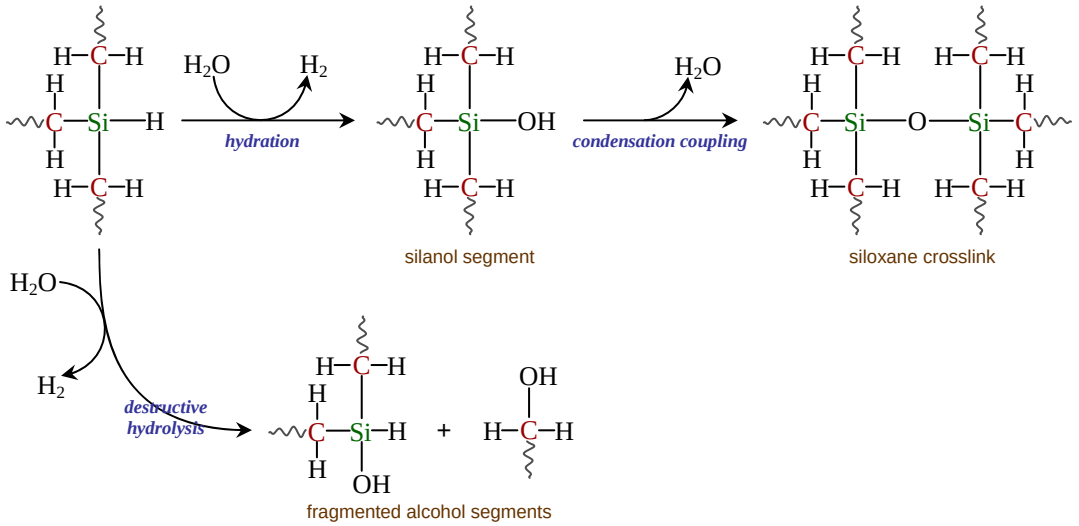

(3) Oxidation of silyl hydride groups along neighboring polymer chains. In a similar fashion as reaction (2), oxidation can proceed along two tremendously different paths . . . siloxane coupling (crosslinking) via condensation or destructively, with the formation of fragmented silanol segments . . .

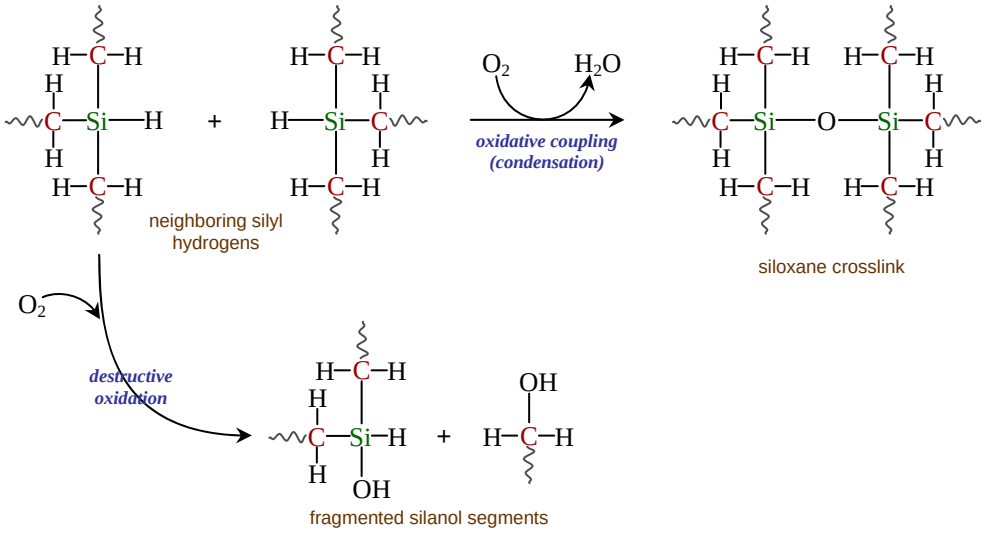

Other than the evolution of dangerous hydrogen, the coupling reactions are not necessarily degradative to the polymer network, but they could conceivably have anomalous effects on the optimal performance of the pre-ceramic material (either path represents aging and unintentional variation within the resin). However, the more damaging effects of chain scission leading to fragmentation of the polymer structure are often catastrophic, though under extremely favorable conditions, these cleavage reactions may be partially reversible, possibly re-coupling the fragments through condensation. Similar analogies to all these processes could easily be defined and illustrated for the silazanes and ureasilazanes. Properly synthesized siloxanes (silicon oxycarbides) are significantly more stable toward these types of

degradative processes and often become the ceramic precursor of choice for lower temperature applications (< ~2500°F), particularly those requiring higher levels of oxidation protection.

Now . . . the intended reactions and processes for SMP-10, as well as all the other pre-ceramic materials, include (a) curing/crosslinking to harden the thermoset polymer and then (b) pyrolysis to convert the hardened polymer into ceramic (SiC in the case of SMP-10). If the freshly synthesized liquid polymer adduct is subjected to high enough temperatures (~300°-400°F), some of the allyl groups will eventually break down into free radicals. Once of few radicals are formed, crosslinking of the polymer (through the attached allyl groups) takes off spontaneously via chain reaction (in shop lingo, the resin 'kicks off'). Alternately, if a small amount of peroxide (1-3%) is mixed into the resin, the peroxide will break down into free radicals at a much lower temperature, kicking off the crosslinking process without the need for high temperature exposure. From a safety perspective, the particular organic peroxides used to crosslink these types of polymers should be free of oxygen and protic hydrogens. They can consist of aliphatics, aromatics or any combination thereof . . . butyl and cumyl peroxides are examples.

Thus, crosslinking between local allyl groups in the SMP-10 system occurs throughout the material and proceeds across three graduating stages . . . (1) *Initiation* (generation of the initial free radicals); (2) *Propagation* (addition of radicals to other local allyl groups as the product molecules grow in size and themselves become newly created radicals); and (3) *Termination* (when the last few radicals combine forming non-radicalized products, the reaction process rapidly falls off) . . .

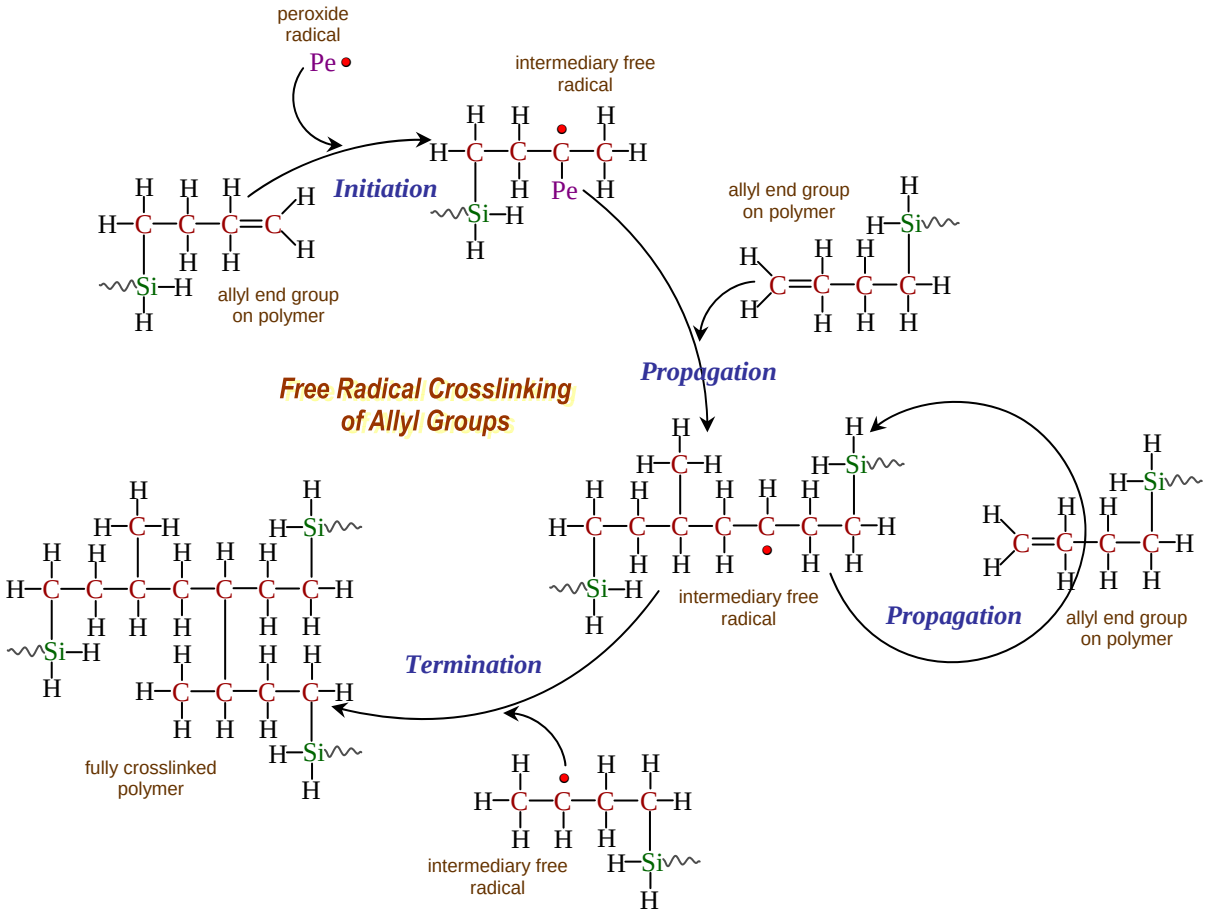

Here, a peroxide radical P• adds to an allyl double bond creating a new, larger radical which itself then adds to another local double bond creating an even larger radical, and so on. It can also be seen from the illustration above that the more allyl groups incorporated into the polymer, the more the Si:C stoichiometric ratio deviates from unity and the more 'carbon rich' the final product will tend to be. Eventually, all the double bonds in the system become saturated (crosslinked) and the chain reaction grinds to a halt. Not shown in this scenario however, are the intermediary propagation steps illustrating the tendency for most newly formed radicals to 'rearrange' in order to form more stable radicals in accordance with the laws of energetics. Ordering of organic free radical stabilities generally runs according to . . .

Stability of Free Radical = Ease of Formation =

benzyl > allyl > tertiary > secondary > primary > methyl > vinyl

This ordering may shed some light on why Starfire workers were able to incorporate allyl groups into the structure but experienced great difficulty with vinyl groups. To avoid confusion, once the allyl double bond is saturated by a radical, the tricarbon group no longer retains its former allylic identity but becomes a secondary group (recall that resonance-stabilized allyl radicals are generated during the original synthesis process when these groups are incorporated onto the polymer end-segments as the *alpha* carbon carries the radical electron – see page 8). However, depending on the local molecular structure, there will be cases where the radical electron can shift to a nearby tertiary carbon, thus lowering the local energy. Inevitably, a radical electron will also shift to the alpha carbon of a local unsaturated allyl group, which can lead to conjugated-assisted crosslinking at the alpha carbon (alpha crosslinks) with preservation of the allyl double bond . . .

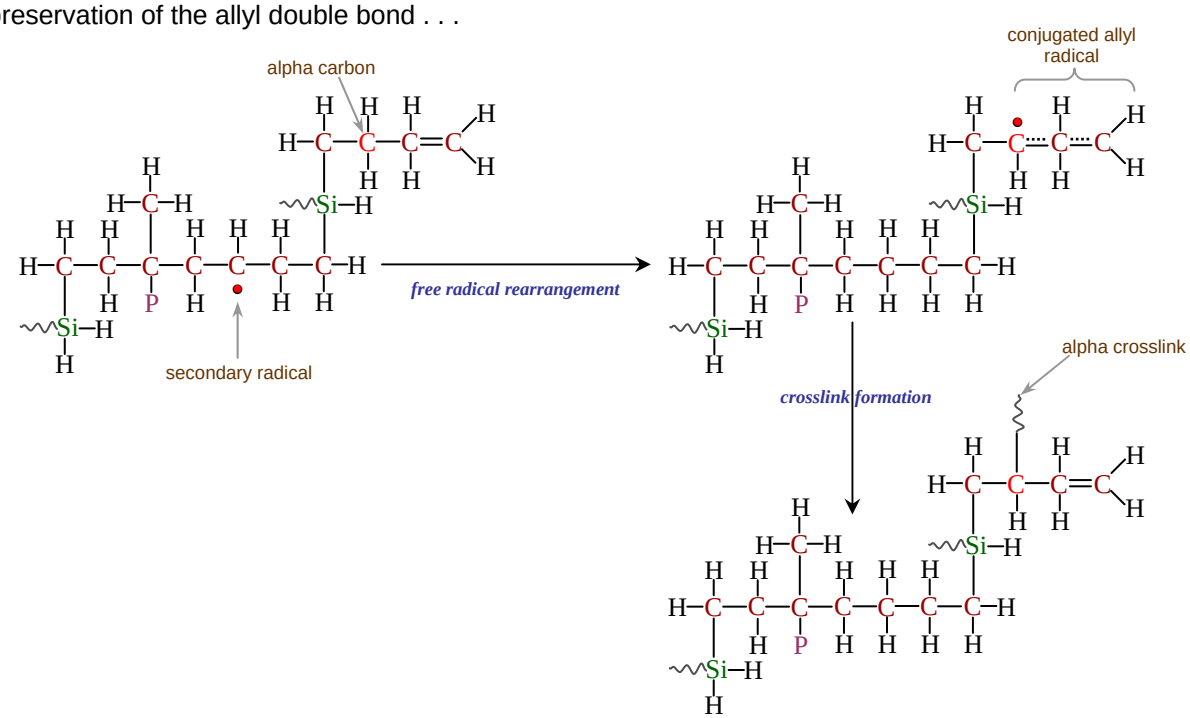

As noted, during this type of crosslinking, the original allyl group remains intact. This double bond can then go ahead and interact with other local segments to form a normal crosslink, as long as steric hindrance permits. In any case, since there is an unrelenting supply of free hydrogen generated throughout the system, a certain fraction of the double bonds will inevitably become saturated with hydrogen as the uncured material ages, which imposes undesirable shelf limits on the resin.

Finally, as the cured polymer is subjected to ever increasing pyrolytic temperatures, it is first converted into an amorphous, glassy form of SiC, designated as a-SiC. This transformation process likely begins around 600°-700° and continues as the temperature is gradually increased, up until about 2000° ± ~200°F. Inert pyrolysis operations kept below this temperature range can be designated as 'low fired' or 'low temperature pyrolysis'. Above the 2000°-2200° range, the a-SiC ceramic begins to crystallize and convert into its face-centered cubic beta form, β-SiC. In this context, inert process temperatures greater than about 2400°-2500°F are understood to mean high fire or high temperature pyrolysis. The structural changes associated with these conversion effects are illustrated below . . .

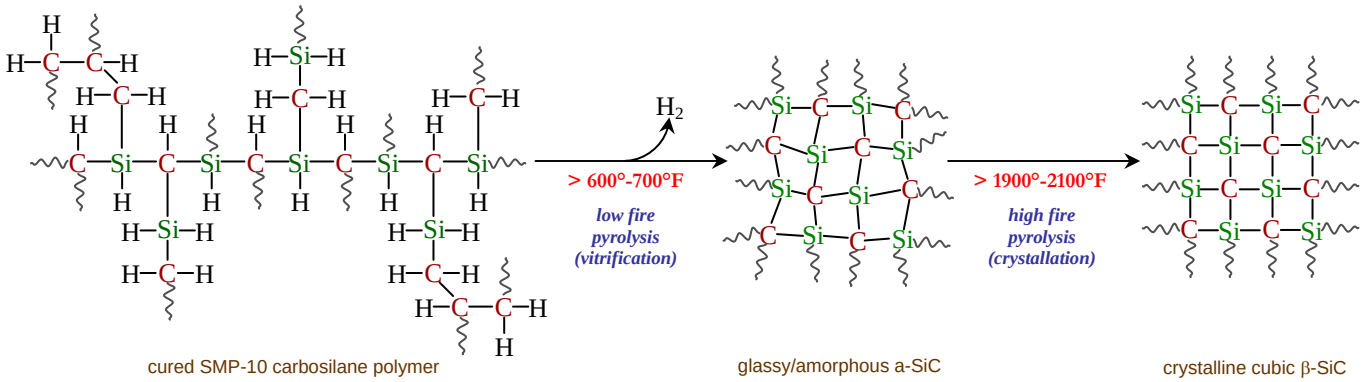

It has been well established that these materials undergo significant volume shrinkage as they are converted into their ceramic forms. As eluded to earlier, the cured polymer will lose about 10-15% of its original volume during conversion into a-SiC and then another 30-40% as the amorphous structure undergoes crystallization. These general ranges also apply to the other pre-ceramics as well. It should be emphasized here that substantial porosity development accompanies these volume changes, particularly when the material converts into the crystalline phase. Thus, applications completely transforming these pre-ceramics into β-SiC, generally require some form of densification-type follow-up procedures to fill up the pores (via CVD/CVI or pre-ceramic polymer impregnation). Undoubtedly, for high temperature applications (>~2500°F), the optimal performance of the pre-ceramics are acquired only after multiple densification treatments (cycles) in which the polymer is applied, cured and pyrolyzed.

The low fired glassy forms of the carbosilanes and ureasilazanes are expected to contain an interconnected micro-porosity network created by the expulsion of hydrogen gas throughout the curing and pyrolysis stages. Due to the nature of these glassy monoliths as they undergo vitrification, a certain level of closed porosity and hermetically sealed voids also form, which later become opened up and expanded during high fire pyrolysis. Even though some workers in the field practice one step procedures with these resinous materials, single shot treatments for critical applications and articles are simply inadequate for coatings, bonded joints or stable high density substrates, unless the goal is a porous product or exposed substrate. Also, it should also be understood that the properties of glassy a-SiC and cubic β-SiC are substantially different. While the bulk densities of a-SiC and β-SiC have been measured to be about ~2.4 and ~3 g/cc respectively, their CTE's run around ~2.5 and ~4+ ppm. Thus, as it is with the various carbon allotropes, not all SiC forms are created equal. Before crystallation of the 'a' phase takes place, mixtures and interfaces of a-SiC and β-SiC behave as two different materials.